DOI: 10.1021/ic1000842

Inorganic Chemistry
Article

Nickel(II) and Palladium(II) Complexes of Azobenzene-Containing Ligands as Dichroic Dyes

Octavia A. Blackburn,[†] Benjamin J. Coe,*[,†] John Fielden,[†] Madeleine Helliwell,[†] Joseph J. W. McDouall,[†] and Michael G. Hutchings[‡]

[†]*School of Chemistry and* [‡]*DyStar UK Ltd, c/o School of Chemistry, University of Manchester, Oxford Road, Manchester M13 9PL, U.K.*

Received January 15, 2010

A large series of complexes has been synthesized with two chelating, Schiff base azobenzene derivatives connected linearly by coordination to a central nickel(II) or palladium(II) ion. These compounds have the general formulas $M^{II}(OC_6H_3\text{-}2\text{-}CHNR\text{-}4\text{-}N{=}NC_6H_4\text{-}4\text{-}CO_2Et)_2$ [M = Ni; R = *n*-Bu (**3c**), *n*-C_6H_{13} (**3d**), *n*-C_8H_{17} (**3e**), *n*-$C_{12}H_{25}$ (**3f**), Ph (**3g**), OH (**3h**), $C_6H_4\text{-}4\text{-}CO_2Et$ (**3i**). M = Pd; R = *i*-Pr (**4a**), *t*-Bu (**4b**), *n*-Bu (**4c**), *n*-C_6H_{13} (**4d**), *n*-C_8H_{17} (**4e**), *n*-$C_{12}H_{25}$ (**4f**), Ph (**4g**)], $M^{II}[OC_6H_3\text{-}2\text{-}CHN(n\text{-}C_8H_{17})\text{-}4\text{-}N{=}NC_6H_4\text{-}4\text{-}CO_2(n\text{-}C_8H_{17})]_2$ [M = Ni (**9**), Pd (**10**)], $M^{II}[OC_6H_3\text{-}2\text{-}CHN(n\text{-}C_8H_{17})\text{-}4\text{-}N{=}NC_6H_4\text{-}4\text{-}C_6H_4\text{-}4\text{-}O(n\text{-}C_7H_{15})]_2$ [M = Ni (**14**), Pd (**15**)], and $M^{II}[OC_6H_3\text{-}2\text{-}CHN(CMe_2)\text{-}4\text{-}N{=}NC_6H_4\text{-}4\text{-}CO_2Et]_2$ [M = Ni (**17**), Pd (**18**); the CMe_2 groups are connected]. These compounds have been characterized by using various physical techniques including ^{1}H NMR spectroscopy and matrix-assisted laser desorption/ionization (MALDI) mass spectrometry. Single-crystal X-ray structures have been obtained for two pro-ligands and five complexes (**3e**, **4e**, **14**, **15**, and **17**). The latter always show a strictly square planar arrangement about the metal center, except for the Ni^{II} complex of a salen-like ligand (**17**). In solution, broadened ^{1}H NMR signals indicate distortions from square planar geometry for the bis-chelate Ni^{II} complexes. Electronic absorption spectroscopy and ZINDO_S (Zerner's intermediate neglect of differential overlap) and TD-DFT (time-dependent density functional theory) calculations show that the lowest energy transition has metal-to-ligand charge-transfer character. The λ_{max} of this band lies in the range of 409−434 nm in dichloromethane, and replacing Ni^{II} with Pd^{II} causes small blue-shifts. Dichroic ratios measured in various liquid crystal hosts show complexation-induced increases with Ni^{II}, but using Pd^{II} has a detrimental effect.

Introduction

Reflective liquid crystal (LC) displays are well suited for applications in emerging technologies such as electronic paper,[1] owing to their ultralow power consumptions achieved through bistability.[2] In this context, much attention has been directed at guest−host LC displays (GH-LCDs) that comprise a dichroic dye dissolved in a LC host. GH-LCDs can achieve excellent brightness combined with wide viewing angles, both critical aspects for device applications. The absorption intensity of a dichroic dye depends on its orientation with respect to the incident light direction. Therefore, when such a dye is ordered within a LC medium, an applied electric field can be used to manipulate the orientation of the molecules and thus change the appearance of the display.[3]

To be suitable for potential GH-LCD applications, a dye must have an especially large dichroic ratio (*DR*). The *DR* is defined as the ratio of the absorbances when illuminated by light polarized parallel ($A_\parallel$) and perpendicular ($A_\perp$) to the LC director. To achieve a sufficiently large *DR*, the transition dipole moment (μ_{12}) of the color-inducing electronic transition must be aligned effectively with the long molecular axis of the dye. The strength and nature of the interactions between the dye molecules and their LC host can also influence the *DR*. In addition, the absorption intensity, solubility in the LC medium, operating temperature, and stability are all important considerations when studying potential dyes for such purposes. The order parameter (*S*) of the dye, defined by eq 1 and related to *DR* by eq 2, is also often used to quantify dichroic properties.

$$S = \frac{A_\parallel - A_\perp}{A_\parallel + 2A_\perp} \quad (1)$$

$$S = \frac{DR - 1}{DR + 2} \quad (2)$$

The two major classes of compound that have attracted the most extensive interest in this field are the classical colorants,

*To whom correspondence should be addressed. E-mail: b.coe@manchester.ac.uk.

(1) (a) Graham-Rowe, D. *Nat. Photonics* **2007**, *1*, 248. (b) Sobel, A. *Nat. Mater.* **2003**, *2*, 643.

(2) (a) Berreman, D. W.; Heffner, W. R. *Appl. Phys. Lett.* **1980**, *37*, 109. (b) Bryan-Brown, G. P.; Brown, C. V.; Jones, J. C.; Wood, E. L.; Sage, I. C.; Brett, P.; Rudin, J. *SID Digest* **1997**, 37.

(3) (a) Heilmeier, G. H.; Zanoni, L. A. *Appl. Phys. Lett.* **1968**, *13*, 91. (b) White, D. L.; Taylor, G. N. *J. Appl. Phys.* **1974**, *45*, 4718.

Published on Web 09/14/2010
© 2010 American Chemical Society

azobenzene and anthraquinone dyes.[4] Previous studies have established that the *S* (and hence also *DR*) value generally increases with the length of the dye molecules, but is inversely related to molecular breadth.[5] Azobenzenes therefore have obvious appeal because of their long, slender shapes which can be expected to lead to good alignment within an LC host.[6] Furthermore, the direction of the intense, low energy $\pi \rightarrow \pi^*$ transition in such dyes is directed approximately along the long molecular axis.

To date, only a handful of studies have specifically addressed the dichroic properties of metal-containing dyes. For example, transition metal dithiolene complexes have found use as modulators of laser light because of their pronounced dichroism in the near-IR region.[7] In other studies, Bruce et al. investigated a series of metal dithiobenzoates and found excellent *DR* values, but poor stability in solution.[8] The objective of this study is to explore the use of square planar coordinated transition metal ions to link two azobenzene chromophores. Given that such complexes are approximately twice the length of the uncoordinated dyes, significant enhancements in *DR* are expected to arise from this approach. Complexes of this general type with nickel have been known for many years,[9] but analogous palladium species are apparently unknown. In addition, previous investigations have involved various closely related complexes of Ni^{II}, Cu^{II}, and other first row d-block metal ions,[10] often as thermotropic liquid crystalline materials,[10b,c,e,g,h,j] but their dichroic behavior has not to our knowledge been examined.

Experimental Section

Materials and Procedures. The compound 4-(*n*-heptoxy)-phenylboronic acid was synthesized according to a published procedure, by using 1-bromo-*n*-heptane in place of 1-bromo-*n*-octane.[11] 2,3-Diamino-2,3-dimethylbutane was synthesized by reduction of 2,3-dinitro-2,3-dimethylbutane according to a literature method.[12] Dichloromethane was dried by distillation over CaH_2 under nitrogen where necessary. All other chemicals were used as supplied by Sigma Aldrich or Alfa Aesar, and the LCs used for dichroism measurements were supplied by Merck and Synthon. Products were dried at room temperature overnight in a vacuum desiccator ($CaSO_4$) or by direct attachment to a high vacuum line for several hours prior to characterization. Representative synthetic and characterization details are reported below, while all the others are included in the Supporting Information.

General Physical Measurements. ^{1}H NMR spectra were recorded on Bruker UltraShield 500, AV 400, or DPX 300 spectrometers, and all shifts are quoted with respect to tetramethylsilane ($SiMe_4$). The fine splitting of phenyl ring AA′BB′ patterns is ignored, and the signals are reported as simple doublets, with *J* values (in Hz) referring to the two most intense peaks. For the assignments of the protons labeled *a*−*d*, see the Discussion section. Electrospray mass spectrometry was performed on a Micromass Platform II at the University of Manchester, while matrix-assisted laser desorption/ionization (MALDI) mass spectra were recorded on a Micromass Tof Spec 2e or an Applied Biosystems Voyager instrument at the EPSRC National Mass Spectrometry Service Centre (U.K.). In cases where clusters of peaks are observed because of the presence of various isotopes, the most intense peak is always quoted. Elemental analyses were performed by the Microanalytical Laboratory, University of Manchester. UV−vis spectra were obtained by using a Shimadzu UV-2401 PC spectrometer, and IR spectra were recorded with pure solids on a Varian Bio-Rad Excalibur series spectrometer. Dichroism measurements were performed on a custom-built Hewlett-Packard machine supplied by HP Research (U.K.). Abbreviations: ald = aldehyde; est = ester.; st = strong; m = medium; vbr = very broad; s = singlet; d = doublet; dd = doublet of doublets; t = triplet; q = quartet; qnt = quintet; spt = septet.

Synthesis of 4-(3-Formyl-4-hydroxyphenylazo)benzoic Acid Ethyl Ester (1). Ethyl-4-aminobenzoate (10.0 g, 60.5 mmol) and hydrochloric acid (37%, 15.2 mL, 0.182 mol) were cooled in an ice bath to below 5 °C. A solution of $NaNO_2$ (4.59 g, 66.5 mmol) in water (30 mL) was added dropwise to the stirred solution, which was then stirred for a further 2 h with the temperature maintained between 0 and 5 °C. This yellow diazonium salt solution was then added slowly to a cooled solution of salicylaldehyde (salal, 6.34 mL, 59.5 mmol) in aqueous NaOH (2 M, 69.5 mL, 0.139 mol), kept below 5 °C for the duration of the addition. The red/orange suspension was stirred with cooling for 1 h, then allowed to warm to room temperature and stirred for 18 h. The orange/brown precipitate was filtered off, washed with water, and recrystallized from ethanol to give an orange solid. Yield 6.46 g (36%). δ_H(400 MHz, $CDCl_3$) 11.39 (1 H, s, OH), 10.04 (1 H, s, CHO), 8.25 (1 H, d, J = 2.4, *a*), 8.22−8.18 (3 H, d + dd, *c* + C_6H_4), 7.93 (2 H, d, J = 8.7, C_6H_4), 7.14 (1 H, d, J = 8.9, *b*), 4.42 (2 H, q, J = 7.1, CH_2), 1.43 (3 H, t, J = 7.1, Me). ν(C═O)$_{est}$ 1705st, ν(C═O)$_{ald}$ 1654st cm^{-1}. Anal. Calcd (%) for $C_{16}H_{14}N_2O_4$: C, 64.42; H, 4.73; N, 9.39. Found: C, 64.39; H, 4.66; N, 9.35. *m*/*z* (−ES): 297.3 $[M - H]^-$.

Synthesis of 4-[4-Hydroxy-3-(*i*-propyliminomethyl)phenylazo]benzoic Acid Ethyl Ester (2aH). Compound **1** (200 mg, 0.670 mmol) and *i*-propylamine (40 mg, 0.677 mmol) were combined in ethanol (40 mL), and a few drops of glacial acetic acid were added. The mixture was heated under reflux for 2 h. Upon cooling, the orange solution was evaporated under reduced pressure, and the resulting solid was triturated with a mixture of diethyl ether and *n*-hexane. The orange solid was filtered off and washed with *n*-hexane. Yield 124 mg (55%). δ_H(500 MHz, $CDCl_3$) 8.41 (1 H, s, CHN),

(4) (a) Bahadur, B. In *Liquid Crystals: Applications and Uses*; Bahadur, B., Ed.; World Scientific: Singapore, 1992; Vol. *3*, pp 65−208. (b) Ivashchenko, A. V. *Dichroic Dyes for Liquid Crystal Displays*; CRC Press: Boca Raton, FL, 1994. (c) Kelly, S. M. *Flat Panel Displays: Advanced Organic Materials*; RSC Publishing: Cambridge, U.K., 2000.

(5) (a) Bahadur, B.; Sarna, R. K.; Bhide, V. G. *Mol. Cryst. Liq. Cryst.* **1981**, *75*, 121. (b) Constant, J.; Raynes, E. P.; Shanks, I. A.; Coates, D.; Gray, G. W.; McDonnell, D. G. *J. Phys. D: Appl. Phys.* **1978**, *11*, 479. (c) Seki, H.; Uchida, T.; Shibata, Y. *Mol. Cryst. Liq. Cryst.* **1986**, *138*, 349.

(6) See for examples: (a) Cognard, J.; Phan, T. H. *Mol. Cryst. Liq. Cryst.* **1981**, *68*, 207. (b) Lackner, A. M.; Sherman, E.; Wong, S.-Y.; Wong, S.-M. *Liq. Cryst.* **1993**, *14*, 763. (c) Matsui, M.; Tanaka, N.; Andoh, N.; Funabiki, K.; Shibata, K.; Muramatsu, H.; Ishigure, Y.; Kohyama, E.; Abe, Y.; Kaneko, M. *Chem. Mater.* **1998**, *10*, 1921.

(7) Marshall, K. L.; Painter, G.; Lotito, K.; Noto, A. G.; Chang, P. *Mol. Cryst. Liq. Cryst.* **2006**, *454*, 47.

(8) Bruce, D. W.; Dunmur, D. A.; Hunt, S. E.; Maitlis, P. M.; Orr, R. *J. Mater. Chem.* **1991**, *1*, 857.

(9) Early examples: (a) LaLancette, E. A.; Eaton, D. R.; Benson, R. E.; Phillips, W. D. *J. Am. Chem. Soc.* **1962**, *84*, 3968. (b) Holm, R. H.; Chakravorty, A.; Dudek, G. O. *J. Am. Chem. Soc.* **1964**, *86*, 379.

(10) (a) Tanaka, M. *Bull. Chem. Soc. Jpn.* **1964**, *37*, 1210. (b) Aiello, I.; Ghedini, M.; Neve, F.; Pucci, D. *Chem. Mater.* **1997**, *9*, 2107. (c) Aiello, I.; Ghedini, M.; La Deda, M.; Pucci, D.; Francescangeli, O. *Eur. J. Inorg. Chem.* **1999**, 1367. (d) Khandar, A. A.; Rezvani, Z.; Nejati, K.; Yanovsky, A. I.; Martinez, J. M. *Acta Chim. Slov.* **2002**, *49*, 733. (e) Nejati, K.; Rezvani, Z. *New J. Chem.* **2003**, *27*, 1665. (f) Rezvani, Z.; Ahar, L. R.; Nejati, K.; Seyedahmadian, S. M. *Acta Chim. Slov.* **2004**, *51*, 675. (g) Rezvani, Z.; Abbasi, A. R.; Nejati, K.; Seyedahmadian, M. *Polyhedron* **2005**, *24*, 1461. (h) Rezvani, Z.; Divband, B.; Abbasi, A. R.; Nejati, K. *Polyhedron* **2006**, *25*, 1915. (i) Liu, J.-N.; Wu, B.-W.; Zhang, B.; Liu, Y.-C. *Turk. J. Chem.* **2006**, *30*, 41. (j) Rezvani, Z.; Ghanea, M. A.; Nejati, K.; Baghaei, S. A. *Polyhedron* **2009**, *28*, 2913.

(11) Lock, S. J.; Goodby, J. W.; Hird, M.; Toyne, K. J. *J. Mater. Chem.* **1995**, *5*, 2175.

(12) Hirel, C.; Vostrikova, K. E.; Pécaut, J.; Ovcharenko, V. I.; Rey, P. *Chem.−Eur. J.* **2001**, *7*, 2007.

8.18 (2 H, d, J = 8.4, C_6H_4), 8.01 (1 H, dd, J_{bc} = 9.4, J_{ac} = 2.3, *c*), 7.92 (1 H, d, J = 2.5, *a*), 7.89 (2 H, d, J = 8.4, C_6H_4), 7.03 (1 H, d, J = 9.0, *b*), 4.41 (2 H, q, J = 7.1, OCH_2), 3.69 (1 H, spt, J = 6.4, C*H*Me$_2$), 1.43 (3 H, t, J = 6.9, CH_2*Me*), 1.37 (6 H, d, J = 6.4, CH*Me*$_2$). ν(C=O) 1703st, ν(C=N) 1622st, ν(C=C) 1603st and 1578st cm^{-1}. Anal. Calcd (%) for $C_{19}H_{21}N_3O_3$: C, 67.24; H, 6.24; N, 12.38. Found: C, 66.98; H, 6.21; N, 12.19. m/z (−ES): 338.2 [M − H]$^-$.

Synthesis of 4-Nitro-*n*-octylbenzoate (5). 4-Nitrobenzoylchloride (10.0 g, 0.054 mol) was dissolved in dry dichloromethane (70 mL) under argon and cooled to 0 °C. A solution of *n*-octanol (8.5 mL, 0.054 mol) and pyridine (38.4 g, 0.485 mol) in dry dichloromethane (20 mL) was added dropwise, and the yellow solution was then left to stir for 16 h. The resulting suspension was filtered, and the filtrate was washed with aqueous NaOH (1 M, 2 × 20 mL), followed by aqueous HCl (1 M, 6 × 20 mL) and then water (3 × 20 mL). The organic layer was dried over $MgSO_4$ and evaporated to give a yellow oil. Yield 14.77 g (98%). δ_H(400 MHz, $CDCl_3$) 8.28 (2 H, d, J = 9.1, C_6H_4), 8.20 (2 H, d, J = 9.1, C_6H_4), 4.36 (2 H, t, J = 6.7, OCH_2), 1.78 (2 H, qnt, J = 6.7, CH_2), 1.45−1.25 (10 H, 5CH_2), 0.87 (3 H, t, J = 6.9, Me). ν(C=O) 1724st, ν(NO_2) 1528st and 1269st cm^{-1}. Anal. Calcd (%) for $C_{15}H_{21}NO_4$: C, 64.50; H, 7.58; N, 5.01. Found: C, 64.50; H, 7.84; N, 5.01. m/z (−ES): 279.3 [M]$^-$.

Synthesis of 4-Amino-*n*-octylbenzoate (6). To a solution of **5** (4.56 g, 0.016 mol) in methanol (100 mL) were added NH_4Cl (1.75 g, 0.033 mol) and zinc powder (7.47 g, 0.114 mol). The gray/brown mixture was heated under reflux for 1 h, then cooled to room temperature and filtered. The filtrate was evaporated to dryness, dissolved in ethyl acetate (100 mL), and washed with water (3 × 70 mL). The ethyl acetate was evaporated to give a solid which was triturated with *n*-hexane to give a pale peach-colored solid. Yield 3.20 g (75%). δ_H(400 MHz, $CDCl_3$) 7.85 (2 H, d, J = 8.8, C_6H_4), 6.64 (2 H, d, J = 8.8, C_6H_4), 4.25 (2 H, t, J = 6.7, OCH_2), 4.03 (2 H, br, NH_2), 1.73 (2 H, qnt, J = 6.7, CH_2), 1.45−1.25 (10 H, 5CH_2), 0.88 (3 H, t, J = 7.1, Me). m/z (−ES): 248.3 [M − H]$^-$. ν(C=O) 1682st cm^{-1}. Note: this material was found by ^{1}H NMR spectroscopy to contain about 5% of the hydroxylamine intermediate; since this could not be removed readily and is not expected to interfere with the reaction to form **7** (see below), the product was used without purification.

Synthesis of 4-(3-Formyl-4-hydroxyphenylazo)benzoic Acid Octyl Ester (7). This compound was prepared in a manner identical to **1**. Addition of $NaNO_2$ (2.52 g, 0.037 mol) to **6** (8.28 g, 0.031 mol) in aqueous HCl (37%, 9.83 mL, 0.10 mol) and water (20 mL) gave a peach-colored solution. The reaction with salal (4.06 g, 0.033 mol) in aqueous NaOH (2 M, 38.0 mL) produced an orange precipitate. The crude product was recrystallized from ethyl acetate and washed with *n*-hexane to give an orange powder. Yield 4.65 g (39%). δ_H(400 MHz, $CDCl_3$) 11.39 (1 H, s, OH), 10.05 (1 H, s, CHO), 8.25 (1 H, d, J = 2.4, *a*), 8.18−8.22 (3 H, d + dd, *c* + C_6H_4), 7.93 (2 H, d, J = 8.8, C_6H_4), 7.14 (1 H, d, J = 8.9, *b*), 4.35 (2 H, t, J = 6.7, OCH_2), 1.80 (2 H, qnt, J = 6.7, CH_2), 1.50−1.25 (10 H, 5CH_2), 0.89 (3 H, t, J = 6.9, Me). ν(C=O)$_{est}$ 1709st, ν(C=O)$_{ald}$ 1666st cm^{-1}. Anal. Calcd (%) for $C_{22}H_{26}N_2O_4$: C, 69.09; H, 6.85; N, 7.32. Found: C, 68.90; H, 6.90; N, 7.28. m/z (−ES): 381.2 [M − H]$^-$.

Synthesis of 4-[4-Hydroxy-3-(*n*-octyliminomethyl)phenylazo]benzoic Acid Octyl Ester (8H). This compound was prepared in a manner identical to **2aH** by using **7** (600 mg, 1.57 mmol) and *n*-octylamine (200 mg, 1.55 mmol) to produce an orange precipitate which was filtered off and washed with ethanol. Yield 700 mg (90%). δ_H(400 MHz, $CDCl_3$) 8.38 (1 H, s, CHN), 8.17 (2 H, d, J = 8.7, C_6H_4), 8.01 (1 H, dd, J_{bc} = 11.5, J_{ac} = 2.5, *c*), 7.92 (1 H, d, J = 2.5, *a*), 7.89 (2 H, d, J = 8.7, C_6H_4), 7.03 (1 H, d, J = 9.0, *b*), 4.34 (2 H, t, J = 6.7, OCH_2), 3.65 (2 H, t, J = 6.5, NCH_2), 1.83−1.70 (4 H, 2CH_2), 1.50−1.20 (20 H, 10CH_2), 0.91−0.85 (6 H, 2Me). ν(C=O) 1701st, ν(C=N) 1631st, ν(C=C) 1605st and 1582st cm^{-1}. Anal. Calcd (%) for $C_{30}H_{43}N_3O_3$: C, 72.99; H, 8.78; N, 8.51. Found: C, 73.12; H, 8.99; N, 8.52. m/z (−ES): 492.2 [M − H]$^-$.

Synthesis of 4-Amino-4′-(*n*-heptoxy)-1,1′-biphenyl (11). 4-Bromoaniline (1.42 g, 8.25 mmol), 4-(*n*-heptoxy)phenylboronic acid (2.15 g, 9.11 mmol), K_2CO_3 (2.86 g, 20.7 mmol), acetone (20 mL), and water (25 mL) were combined in a Schlenk tube, and the mixture was degassed by two freeze−pump−thaw cycles. The addition of a solution of $Pd^{II}(OAc)_2$ (3.7 mg, 0.016 mmol) in acetone (5 mL) via a syringe was followed by three further freeze−pump−thaw cycles. The mixture was heated under argon at 65 °C for 4 h, then cooled to room temperature and extracted with diethyl ether (3 × 150 mL). The combined extracts were washed with water (2 × 150 mL), dried over $MgSO_4$ and evaporated to give a gray solid. Repeated trituration with ethanol gave a white solid. Yield 1.65 g (64%). δ_H(400 MHz, $CDCl_3$) 7.44 (2 H, d, J = 8.9, C_6H_4), 7.36 (2 H, d, J = 8.7, C_6H_4), 6.93 (2 H, d, J = 8.9, C_6H_4), 6.74 (2 H, d, J = 8.7, C_6H_4), 3.98 (2 H, t, J = 6.6, OCH_2), 3.68 (2 H, br, NH_2), 1.80 (2 H, qnt, J = 6.7, CH_2) 1.51−1.25 (8 H, 4CH_2), 0.90 (3 H, t, J = 7.0, Me). Anal. Calcd (%) for $C_{19}H_{25}NO$: C, 80.52; H, 8.89; N, 4.94. Found: C, 80.17; H, 9.02; N, 4.79. m/z (+ES): 284.3 [M + H]$^+$.

Synthesis of 4-(3-Formyl-4-hydroxyphenylazo)-4′-(*n*-heptoxy)-1,1′-biphenyl (12). This compound was prepared in a manner identical to **1**. The addition of $NaNO_2$ (0.40 g, 5.80 mmol) to **11** (1.50 g, 5.29 mmol) in aqueous HCl (37%, 1.6 mL, 0.16 mol) and water (10 mL) gave a yellow suspension. Coupling with salal (0.65 g, 5.32 mmol) in aqueous NaOH (2 M, 6.1 mL) produced a green/brown precipitate. Purification was achieved by trituration with diethyl ether followed by column chromatography on silica gel eluting with dichloromethane. The major yellow fraction was collected and evaporated to dryness under vacuum to afford a yellow solid. Yield 1.39 g (63%). δ_H(400 MHz, $(CD_3)_2SO$) 10.23 (1 H, s, CHO), 7.98 (1 H, d, J = 2.8, *a*), 7.85 (1 H, dd, J_{bc} = 9.3, J_{ac} = 2.8, *c*), 7.80 (2 H, d, J = 8.8, C_6H_4), 7.75 (2 H, d, J = 8.8, C_6H_4), 7.67 (2 H, d, J = 8.8, C_6H_4), 7.02 (2 H, d, J = 8.8, C_6H_4), 6.64 (1 H, d, J = 9.3, *b*), 4.01 (2 H, t, J = 6.4, OCH_2), 1.73 (2 H, qnt, J = 6.7, CH_2), 1.46−1.22 (8 H, 4CH_2), 0.87 (3 H, t, J = 7.0, Me). ν(C=O) 1655st cm^{-1}. Anal. Calcd (%) for $C_{26}H_{28}N_2O_3$: C, 74.97; H, 6.78; N, 6.73. Found: C, 74.62; H, 7.22; N, 6.66. m/z (−ES): 415.3 [M − H]$^-$.

Synthesis of 4-[4-Hydroxy-3-(*n*-octyliminomethyl)phenylazo]-4′-(*n*-heptoxy)-1,1′-biphenyl (13H). This compound was prepared in a manner identical to **2aH** by using **12** (500 mg, 1.20 mmol) and *n*-octylamine (155 mg, 1.20 mmol) to produce an orange precipitate which was filtered off and washed with ethanol. Yield 485 mg (76%). δ_H(400 MHz, $CDCl_3$) 14.43 (1 H, br, OH), 8.40 (1 H, s, CHN), 7.99 (1 H, dd, J_{bc} = 8.9, J_{ac} = 2.5, *c*), 7.95−7.89 (3 H, C_6H_4 + *a*), 7.69 (2 H, d, J = 8.8, C_6H_4), 7.59 (2 H, d, J = 8.9, C_6H_4), 7.04 (1 H, d, J = 8.9, *b*), 6.99 (2 H, d, J = 8.9, C_6H_4), 4.01 (2 H, t, J = 6.6, OCH_2), 3.64 (2 H, t, J = 6.7, NCH_2), 1.86−1.69 (4 H, 2CH_2), 1.52−1.22 (18 H, 9CH_2), 0.94−0.85 (6 H, 2Me). ν(C=N) 1636st, ν(C=C) 1604st and 1582st cm^{-1}. Anal. Calcd (%) for $C_{34}H_{45}N_3O_2$: C, 77.38; H, 8.59; N, 7.96. Found: C, 77.53; H, 8.45; N, 7.69. m/z (−ES): 526.4 [M − H]$^-$.

Synthesis of 1,1,2,2-Tetramethyl-*N*,*N*′-Di{2-hydroxy-5-[4-(ethoxycarbonyl)phenylazo]benzylidine}ethane-1,2-diamine (16H$_2$). This compound was prepared in a manner similar to **2aH** by using **1** (206 mg, 0.691 mmol) and 2,3-diamino-2,3-dimethylbutane (40 mg, 0.344 mmol) and ethanol (40 mL). The mixture was heated under reflux for 5 h. After cooling, the precipitate was filtered off to give an orange solid. Yield 105 mg (45%). δ_H(400 MHz, $CDCl_3$) 14.68 (2 H, s, 2OH), 8.47 (2 H, s, 2CHN), 8.17 (4 H, d, J = 8.7, 2C_6H_4), 8.01 (2 H, dd, J_{bc} = 9.0, J_{ac} = 2.4, 2*c*), 7.96 (2 H, d, J = 2.4, 2*a*), 7.87 (4 H, d, J = 8.7, 2C_6H_4), 7.05 (2 H, d, J = 9.0, 2*b*), 4.41 (4 H, q, J = 7.1, 2OCH_2), 1.49 (12 H, s, 4Me), 1.43 (6 H, t, J = 7.1, 2Me$_{est}$). ν(C=O) 1740st, ν(C=N) 1622st, ν(C=C) 1603st and 1589st cm^{-1}. Anal. Calcd (%) for $C_{38}H_{40}N_6O_6$: C, 67.44; H, 5.96; N, 12.42. Found: C, 67.40; H, 5.94; N, 12.33. m/z (−ES): 675.7 [M − H]$^-$.

Synthesis of $Ni^{II}(2c)_2$ (3c). The pro-ligand **2cH** (70 mg, 0.198 mmol) and $Ni^{II}(OAc)_2\cdot 4H_2O$ (25 mg, 0.100 mmol) were combined in ethanol (20 mL), and the mixture was heated under reflux for 2 h. Upon cooling, the resulting precipitate was filtered off and washed with ethanol, then purified by recrystallization from dichloromethane to give a brown solid. Yield 37 mg (49%). δ_H(500 MHz, $CDCl_3$) 8.91 (2 H, br, 2CHN), 8.16 (4 H, d, J = 8.6, $2C_6H_4$), 7.89 (2 H, dd, J_{bc} = 8.8, 2*c*), 7.88 (2 H, d, J = 2.4, 2*a*), 7.84 (4 H, d, J = 8.5, $2C_6H_4$), 6.65 (2 H, d, J = 8.9, 2*b*), 4.41 (4 H, q, J = 7.4, $2OCH_2$), 3.74 (4 H, br, $2NCH_2$), 1.93 (4 H, qnt, J = 7.3, $2CH_2$), 1.53 (4 H, qnt, J = 7.5, $2CH_2$), 1.43 (6 H, t, J = 7.1, $2Me_{est}$), 1.03 (6 H, t, J = 7.4, 2Me). ν(C=O) 1703st, ν(C=N) 1612st, ν(C=C) 1599st cm^{-1}. Anal. Calcd (%) for $C_{40}H_{44}N_6NiO_6$: C, 62.92; H, 5.81; N, 11.01. Found: C, 62.50; H, 5.53; N, 10.82. *m*/*z* (+ES): 785.5 $[M + Na]^+$.

Synthesis of $Pd^{II}(2a)_2$ (4a). The pro-ligand **2aH** (53 mg, 0.156 mmol) and $Pd^{II}(OAc)_2$ (21 mg, 0.094 mmol) were combined in ethanol (15 mL) and heated under reflux for 24 h. After cooling to room temperature, the resulting precipitate was filtered off and washed with ethanol to give a brown solid which was purified by reprecipitation from a dichloromethane solution with *n*-hexane followed by filtration of a dichloromethane solution through Celite. Removal of the solvent under vacuum gave an orange solid. Yield 20 mg (32%). δ_H(500 MHz, $CDCl_3$) 8.17 (4 H, d, J = 8.5, $2C_6H_4$), 8.00 (2 H, d, J = 2.2, 2*a*), 7.97 (2 H, dd, J_{bc} = 9.2, J_{ac} = 2.4, 2*c*), 7.87 (4 H, d, J = 8.5, $2C_6H_4$), 7.80 (2 H, s, 2CHN), 6.98 (2 H, d, J = 9.0, 2*b*), 4.83 (2 H, spt, J = 6.6, $2CHMe_2$), 4.41 (4 H, q, J = 7.1, $2OCH_2$), 1.47 (12 H, d, J = 6.6, $2CHMe_2$), 1.43 (6 H, t, J = 7.1, $2Me_{est}$). ν(C=O) 1711st, ν(C=N) 1626st, ν(C=C) 1599st cm^{-1}. Anal. Calcd (%) for $C_{38}H_{40}N_6O_6Pd\cdot 0.1CH_2Cl_2$: C, 57.80; H, 5.12; N, 10.62. Found: C, 57.39; H, 4.90; N, 10.39. *m*/*z* (+MALDI): 781 $[M - 2H]^+$.

Synthesis of $Ni^{II}(8)_2$ (9). The pro-ligand **8H** (100 mg, 0.203 mmol) and $Ni^{II}(OAc)_2\cdot 4H_2O$ (25 mg, 0.100 mmol) were combined in ethanol (20 mL) and heated under reflux for 2 h. The resulting light brown precipitate was filtered off, washed with ethanol, and recrystallized from dichloromethane/methanol. Yield 70 mg (67%). δ_H(400 MHz, $CDCl_3$) about 9.4 (2 H, vbr, 2CHN), 8.15 (4 H, d, J = 8.6, $2C_6H_4$), 7.97 (2 H, br, 2*c*), 7.89 (2 H, br, 2*a*), 7.83 (4 H, d, J = 8.4, $2C_6H_4$), 6.61 (2 H, d, J = 9.1, 2*b*), 4.34 (4 H, t, J = 6.7, $2OCH_2$), 4.02 (4 H, br, $2NCH_2$), 1.93 (4 H, br, $2CH_2$), 1.79 (4 H, qnt, J = 7.6, $2CH_2$), 1.52−1.22 (40 H, $20CH_2$), 0.93−0.83 (12 H, 4Me). ν(C=O) 1709st, ν(C=N) 1612st, ν(C=C) 1597st cm^{-1}. Anal. Calcd (%) for $C_{60}H_{84}N_6NiO_6$: C, 69.02; H, 8.11; N, 8.05. Found: C, 68.68; H, 8.19; N, 7.93. *m*/*z* (+MALDI): 1043.4 $[M - H]^+$.

Synthesis of $Pd^{II}(8)_2$ (10). The pro-ligand **8H** (100 mg, 0.203 mmol) and $Pd^{II}(OAc)_2$ (27 mg, 0.120 mmol) were combined in ethanol (20 mL) and heated under reflux for 24 h. The resultant brown precipitate was filtered off, washed with ethanol, and purified by column chromatography on silica gel eluting with dichloromethane. The major orange fraction was collected and evaporated to dryness under vacuum to give an orange solid. Yield 60 mg (54%). δ_H(400 MHz, $CDCl_3$) 8.16 (4 H, d, J = 8.5, $2C_6H_4$), 7.94−8.01 (4 H, 2*a* + 2*c*), 7.87 (4 H, d, J = 8.5, $2C_6H_4$), 7.78 (2 H, s, 2CHN), 6.95 (2 H, d, J = 8.7, 2*b*), 4.84 (4 H, t, J = 6.7, $2OCH_2$), 3.77 (4 H, t, J = 7.5, $2NCH_2$), 1.74−1.88 (8 H, 2qnt, $4CH_2$), 1.17−1.51 (40 H, $20CH_2$), 0.93−0.83 (12 H, 4Me). ν(C=O) 1705st, ν(C=N) 1622st, ν(C=C) 1599st cm^{-1}. Anal. Calcd (%) for $C_{60}H_{84}N_6O_6Pd$: C, 66.01; H, 7.76; N, 7.70. Found: C, 65.01; H, 7.99; N, 7.43. *m*/*z* (+MALDI): 1091.5 $[M]^+$.

Synthesis of $Ni^{II}(13)_2$ (14). The pro-ligand **13H** (80 mg, 0.152 mmol) and $Ni^{II}(OAc)_2\cdot 4H_2O$ (19 mg, 0.076 mmol) were combined in ethanol (20 mL) and heated under reflux for 2 h. The resulting dark green precipitate was filtered off, washed with ethanol and recrystallized from dichloromethane. Yield 58 mg (69%). δ_H(400 MHz, $CDCl_3$) about 9.3 (2 H, vbr, 2CHN), 7.93 (2 H, d, J = 9.4, 2*c*), 7.89−7.82 (6 H, $2C_6H_4$ + 2*a*), 7.67 (4 H, d, J = 8.6, $2C_6H_4$), 7.59 (4 H, d, J = 8.7, $2C_6H_4$), 6.99 (4 H, d, J = 8.7, $2C_6H_4$), 6.63 (2 H, d, J = 9.1, 2*b*), 4.01 (4 H, t, J = 6.7, $2OCH_2$), 3.89 (4 H, br, $2NCH_2$), 1.94 (4 H, br, $2CH_2$), 1.81 (4 H, qnt, J = 8.0, $2CH_2$), 1.53−1.23 (36 H, $18CH_2$), 0.93−0.84 (12 H, 4Me). ν(C=N)/ν(C=C) 1609st cm^{-1}. Anal. Calcd (%) for $C_{68}H_{88}N_6NiO_4$: C, 73.44; H, 7.98; N, 7.56. Found: C, 73.83; H, 8.23; N, 7.45. *m*/*z* (+MALDI): 1112 $[M]^+$. Diffraction-quality crystals were obtained by slow evaporation of a dichloromethane solution at room temperature.

Synthesis of $Pd^{II}(13)_2$ (15). This compound was prepared and purified in a manner identical to **14** by using $Pd^{II}(OAc)_2$ (17 mg, 0.076 mmol) in place of $Ni^{II}(OAc)_2\cdot 4H_2O$ and a reflux time of 24 h, giving a red/brown solid. Yield 47 mg (54%). δ_H(400 MHz, $CDCl_3$) 7.98 (2 H, dd, J_{bc} = 9.2, J_{ac} = 2.8, 2*c*), 7.93−7.87 (6 H, $2C_6H_4$ + 2*a*), 7.76 (2 H, s, 2CHN), 7.67 (4 H, d, J = 8.7, $2C_6H_4$), 7.59 (4 H, d, J = 8.8, $2C_6H_4$), 6.99 (4 H, d, J = 8.8, $2C_6H_4$), 6.95 (2 H, d, J = 9.1, 2*b*), 4.01 (4 H, t, J = 6.7, $2OCH_2$), 3.76 (4 H, t, J = 7.3, $2NCH_2$), 1.88−1.77 (8 H, $4CH_2$), 1.53−1.21 (36 H, $18CH_2$), 0.93−0.85 (12 H, 4Me). ν(C=N) 1618st, ν(C=C) 1603st cm^{-1}. Anal. Calcd (%) for $C_{68}H_{88}N_6O_4Pd$: C, 70.42; H, 7.65; N, 7.25. Found: C, 70.23; H, 7.81; N, 7.06. *m*/*z* (+MALDI): 1160 $[M + H]^+$. Diffraction-quality crystals were obtained by layering of ethanol on top of a chloroform solution at room temperature.

Synthesis of $Ni^{II}(16)_2$ (17). The pro-ligand **$16H_2$** (30 mg, 0.044 mmol) and $Ni^{II}(OAc)_2\cdot 4H_2O$ (11 mg, 0.044 mmol) were combined in ethanol (15 mL) and heated under reflux for 2 h. The resulting red precipitate was filtered off and washed with ethanol. Yield 17 mg (53%). δ_H(400 MHz, $CDCl_3$) 8.16 (4 H, d, J = 8.8, $2C_6H_4$), 7.97 (2 H, dd, J_{bc} = 9.2, J_{ac} = 2.5, 2*c*), 7.92 (2 H, d, J = 2.5, 2*a*), 7.85 (4 H, d, J = 8.8, $2C_6H_4$), 7.67 (2 H, s, 2CHN), 7.14 (2 H, d, J = 9.2, 2*b*), 4.41 (4 H, q, J = 7.1, $2OCH_2$), 1.54 (12 H, s, 4Me), 1.42 (6 H, t, J = 7.1, $2Me_{est}$). ν(C=O) 1740st, ν(C=N) 1606st, ν(C=C) 1597st cm^{-1}. Anal. Calcd (%) for $C_{38}H_{38}N_6NiO_6$: C, 62.23; H, 5.22; N, 11.46. Found: C, 62.05; H, 5.48; N, 10.83. *m*/*z* (+ES): 732.6 $[M]^+$, 755.6 $[M + Na]^+$. Diffraction-quality crystals were obtained by layering of ethanol on top of a chloroform solution at room temperature.

Synthesis of $Pd^{II}(16)_2$ (18). The pro-ligand **$16H_2$** (40 mg, 0.059 mmol) and $Pd^{II}(OAc)_2$ (14 mg, 0.062 mmol) were combined in ethanol (20 mL) and heated under reflux for 24 h. The resultant brown precipitate was filtered off, washed with ethanol and purified by reprecipitation from a dichloromethane solution with *n*-hexane followed by filtration of a dichloromethane solution through Celite. Removal of the solvent under vacuum gave an orange solid. Yield 10 mg (22%). δ_H(400 MHz, $CDCl_3$) 8.17 (4 H, d, J = 8.7, $2C_6H_4$), 8.08 (2 H, dd, J_{bc} = 9.2, J_{ac} = 2.5, 2*c*), 8.04 (2 H, d, J = 2.5, 2*a*), 7.96 (2 H, s, 2CHN), 7.86 (4 H, d, J = 8.6, $2C_6H_4$), 7.28 (2 H, d, J = 9.2, 2*b*), 4.41 (4 H, q, J = 7.1, $2OCH_2$), 1.59 (12 H, s, 4Me), 1.42 (6 H, t, J = 7.1, $2Me_{est}$). ν(C=O) 1720st, ν(C=N)/ν(C=C) 1597st cm^{-1}. Anal. Calcd (%) for $C_{38}H_{38}N_6O_6Pd$: C, 58.43; H, 4.90; N, 10.76. Found: C, 58.32; H, 4.94; N, 10.54. *m*/*z* (−ES): 779.2 $[M - H]^-$.

X-ray Crystallography. Crystal structures of the pro-ligands **2eH** and **2gH** and of the complexes **3e**, **4e**, **14**, **15**, and **17** have been obtained. Data were collected on Oxford Diffraction XCalibur 2 or Bruker APEX II CCD X-ray diffractometers by using MoK_α radiation (λ = 0.71073 Å), and the data were processed by using the Oxford Diffraction CrysAlis RED[13] or Bruker SAINT[14] software packages with an absorption correction for **4e** carried out with SADABS.[15] The structures were solved by direct methods by using SIR-92[16] via WinGX,[17] or SHELXS-97,[18] and refined by full-matrix least-squares on all

(13) *CrysAlis RED*, Version 1.171.32.4; Oxford Diffraction Ltd.: Yarnton, Oxfordshire, U.K., 2006.
(14) *SAINT*, Version 6.45; Bruker AXS Inc.: Madison: WI, 2003.
(15) *SADABS*, Version 2.10; Bruker AXS Inc.: Madison: WI, 2003.
(16) Altomare, A.; Cascarano, G.; Giacovazzo, C.; Guagliardi, A.; Burla, M. C.; Polidori, G.; Camalli, M. *J. Appl. Crystallogr.* **1994**, *27*, 435.
(17) Farrugia, L. J. *J. Appl. Crystallogr.* **1999**, *32*, 837.
(18) Sheldrick, G. M. *Acta Crystallogr., Sect. A* **1990**, *46*, 467.

Table 1. Crystallographic Data and Refinement Details for the Pro-Ligands **2eH** and **2gH** and the Complexes **3e**, **4e**, **14**, **15**, and **17**

	2eH	2gH	3e	4e	14	15	17
empirical formula	$C_{24}H_{31}N_3O_3$	$C_{22}H_{19}N_3O_3$	$C_{48}H_{60}N_6NiO_6$	$C_{48}H_{60}N_6O_6Pd$	$C_{68}H_{88}N_6NiO_4$	$C_{68}H_{88}N_6O_4Pd$	$C_{38}H_{38}N_6NiO_6$
fw	409.52	373.40	875.73	923.42	1112.15	1159.84	733.45
cryst syst	triclinic	triclinic	triclinic	triclinic	triclinic	triclinic	monoclinic
space group	$P\bar{1}$	$P\bar{1}$	$P\bar{1}$	$P\bar{1}$	$P\bar{1}$	$P\bar{1}$	$P2_1/c$
a/Å	5.6096(17)	6.4080(12)	8.463(16)	8.856(9)	12.090(1)	10.0155(16)	18.447(2)
b/Å	8.297(3)	11.809(2)	9.997(17)	8.927(10)	16.281(2)	10.6712(16)	12.3599(15)
c/Å	24.364(7)	12.790(2)	14.83(3)	15.326(16)	16.502(2)	15.734(3)	15.3860(18)
α/deg	90.544(5)	109.641(4)	76.12(3)	87.95(2)	111.935(11)	93.604(3)	
β/deg	90.773(5)	91.511(4)	84.69(4)	74.088(16)	92.051(9)	106.048(4)	105.989(2)
γ/deg	105.117(5)	94.302(4)	69.92(3)	83.86(2)	94.684(9)	108.118(4)	
U/Å^3	1094.5(6)	907.5(3)	1144(3)	1159(2)	2995.3(6)	1515.4(4)	3372.4(7)
Z	2	2	1	1	2	1	4
T/K	100(2)	100(2)	230(2)	100(2)	100(2)	100(2)	100(2)
μ/mm^{-1}	0.083	0.093	0.478	0.454	0.378	0.359	0.634
cryst size/mm	0.50 × 0.50 × 0.06	0.65 × 0.10 × 0.06	0.45 × 0.35 × 0.10	0.60 × 0.10 × 0.02	0.40 × 0.20 × 0.05	0.40 × 0.08 × 0.05	0.18 × 0.18 × 0.05
appearance	orange plate	orange needle	orange plate	orange plate	yellow rhombic plate	orange needle	orange plate
reflns collected	7832	4782	5819	5567	15493	7646	20453
independent reflns (R_{int})	3827 (0.0607)	3155 (0.0651)	3973 (0.0943)	2416 (0.1184)	8552 (0.0638)	5264 (0.0827)	4847 (0.0777)
reflns with $I > 2\sigma(I)$	2621	1589	2592	1810	3912	3588	3943
GOF on F^2	0.970	0.794	0.875	1.058	0.856	0.907	1.212
final R1, wR2 [$I > 2\sigma(I)$]	0.0477, 0.0997	0.0559, 0.1028	0.0539, 0.1137	0.0785, 0.1659	0.0486, 0.1223	0.0661, 0.1155	0.0713, 0.1028
(all data)	0.0757, 0.1099	0.1075, 0.1165	0.0790, 0.1228	0.1089, 0.1938	0.1171, 0.1561	0.0994, 0.1276	0.0971, 0.1106
peak and hole/eÅ^{-3}	0.260, −0.174	0.266, −0.218	0.369, −0.344	1.080, −0.866	0.318, −0.505	0.834, −0.488	0.489, −0.487

F_o^2 data using SHELXL-97.[19] All other calculations were carried out by using the SHELXTL package.[20] All non-hydrogen atoms were refined anisotropically, and hydrogen atoms were included in idealized positions by using the riding model, with thermal parameters 1.2 times those of aromatic parent carbon atoms, and 1.5 times those of methyl parent carbons. For **14** and **17**, the data were cut at 0.9 Å resolution, and for **4e**, they were cut at 1 Å, because the crystals diffracted rather weakly at high angles. The complexes **3e**, **4e**, and **15** all show crystallographic inversion centers at the metal atom. Crystallographic data and refinement details are presented in Table 1.

Dichroic Ratio Measurements. *DR* values were measured by using custom equipment and software courtesy of Hewlett-Packard Ltd. LC cells were purchased from Linkam Scientific, and syringe filters were purchased from Fisher Scientific U.K. Ltd. A dye (approximately 1% by weight) was dissolved in the LC by stirring above the clearing temperature for approximately 16 h. Slow cooling was followed by filtration through a PTFE syringe filter of pore size 0.2 μm to remove any undissolved dye. Glass cells, with a 5 μm wide gap and rubbed polyimide surface to give antiparallel alignment, were filled by capillary action above the clearing temperature of the LC and allowed to cool. The absorption of the solution was measured parallel and perpendicular to the direction of rubbing, and the DR ($A_\perp/A_\parallel$) was calculated at the absorption maximum. A cell containing only the LC was used as a reference. Quoted values are averages of at least two separate measurements. The error on each value is approximated to be a maximum of ±10%, as determined from repeated measurements with a standard black dye (Merck).

Theoretical Calculations. ZINDO (Zerner's intermediate neglect of differential overlap) calculations were carried out on the complete molecules **2eH** and **3e** by using the Gaussian 03 suite of programs,[21] with the crystallographically determined geometries. The first 50 excited states were obtained, covering wavelength ranges of approximately 167−495 nm (**2eH**) and 211−616 nm (**3e**). ZINDO calculations were also performed with structures optimized at the semiempirical ZNDDO_2 level, as implemented in the ORCA programs.[22] Structure optimization (BP86/Def2-SVP)[23,24] and time-dependent density functional calculations were also carried out on model systems by using Gaussian 03.[21] The first 60 excited states were obtained using B3LYP[25] and MPW1PW91[26] exchange-correlation functionals and Def2-SVP basis sets, covering wavelength ranges of approximately 159−511 nm (pro-ligand) and 243−728 nm (Ni^{II} complex). The UV−vis absorption spectra were simulated by using the GaussSum program.[27]

Results and Discussion

Synthesis. The chemistry used to access the ethyl ester-functionalized pro-ligands **2aH**−**iH** and their corresponding Ni^{II} and Pd^{II} complexes is shown in Scheme 1.

(19) Sheldrick, G. M. *SHELXL 97, Program for Crystal Structure Analysis*, Release 97-2; University of Göttingen: Göttingen, Germany, 1997.
(20) *SHELXTL*, Version 6.10; Bruker AXS Inc.: Madison: WI, 2000.
(21) Frisch, M. J.; Trucks, G. W.; Schlegel, H. B.; Scuseria, G. E.; Robb, M. A.; Cheeseman, V. G.; Montgomery, J. A., Vreven, Jr. T.; Kudin, K. N.; Burant, J. C.; Millam, J. M.; Iyengar, S. S.; Tomasi, J.; Barone, V.; Mennucci, B.; Cossi, M.; Scalmani, G.; Rega, N.; Petersson, G. A.; Nakatsuji, H.; Hada, M.; Ehara, M.; Toyota, K.; Fukuda, R.; Hasegawa, J.; Ishida, M.; Nakajima, T.; Honda, Y.; Kitao, O.; Nakai, H.; Klene, M.; Li, X.; Knox, J. E.; Hratchian, H. P.; Cross, J. B.; Adamo, C.; Jaramillo, J.; Gomperts, R.; Stratmann, R. E.; Yazyev, O.; Austin, A. J.; Cammi, R.; Pomelli, C.; Ochterski, J. W.; Ayala, P. Y.; Morokuma, K.; Voth, G. A.; Salvador, P.; Dannenberg, J. J.; Zakrzewski, V. G.; Dapprich, S.; Daniels, A. D.; Strain, M. C.; Farkas, O.; Malick, D. K.; Rabuck, A. D.; Raghavachari, K.; Foresman, J. B.; Ortiz, J. V.; Cui, Q.; Baboul, A. G.; Clifford, S.; Cioslowski, J.; Stefanov, B. B.; Liu, G.; Liashenko, A.; Piskorz, P.; Komaromi, I.; Martin, R. L.; Fox, D. J.; Keith, T.; Al-Laham, M. A.; Peng, C. Y.; Nanayakkara, A.; Challacombe, M.; Gill, P. M. W.; Johnson, B.; Chen, W.; Wong, M. W.; Gonzalez, C.; Pople, J. A. *Gaussian 03*, Revision C.02; Gaussian, Inc.: Wallingford, CT, 2004.
(22) Neese, F. *ORCA - an ab initio, Density Functional and Semiempirical Program Package*, v. 2.6-35; Universität Bonn: Bonn, Germany, 2007.
(23) (a) Becke, A. D. *Phys. Rev. A* **1988**, *38*, 3098. (b) Perdew, J. P. *Phys. Rev. B* **1986**, *33*, 8822.
(24) Weigend, F.; Ahlrichs, R. *Phys. Chem. Chem. Phys.* **2005**, *7*, 3297.
(25) Becke, A. D. *J. Chem. Phys.* **1993**, *98*, 5648.
(26) Adamo, C.; Barone, V. *J. Chem. Phys.* **1998**, *108*, 664.
(27) O'Boyle, N. M.; Tenderholt, A. L.; Langner, K. M. *J. Comput. Chem.* **2008**, *29*, 839.

Scheme 1. Syntheses of the New Ethyl Ester-Functionalized Pro-Ligands **2aH**−**iH** and Their Ni/Pd Complexes

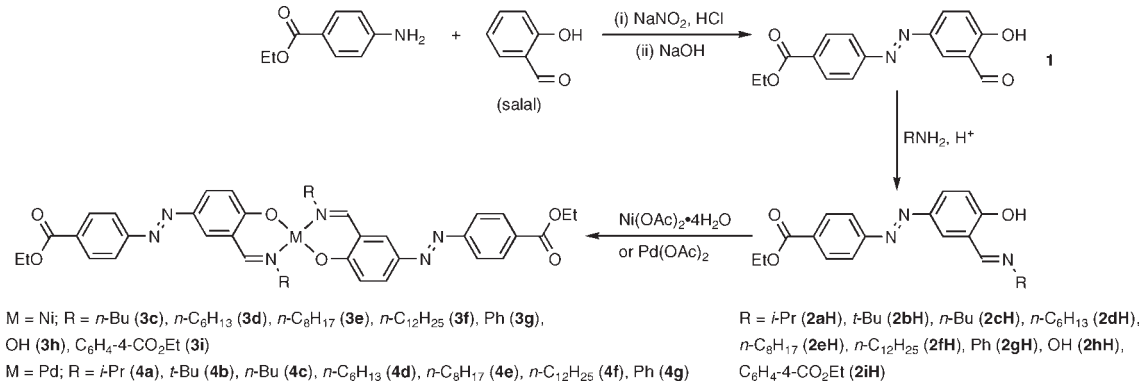

Scheme 2. Syntheses of the New *n*-Octyl Ester-Functionalized Pro-Ligand **8H** and Its Ni/Pd Complexes

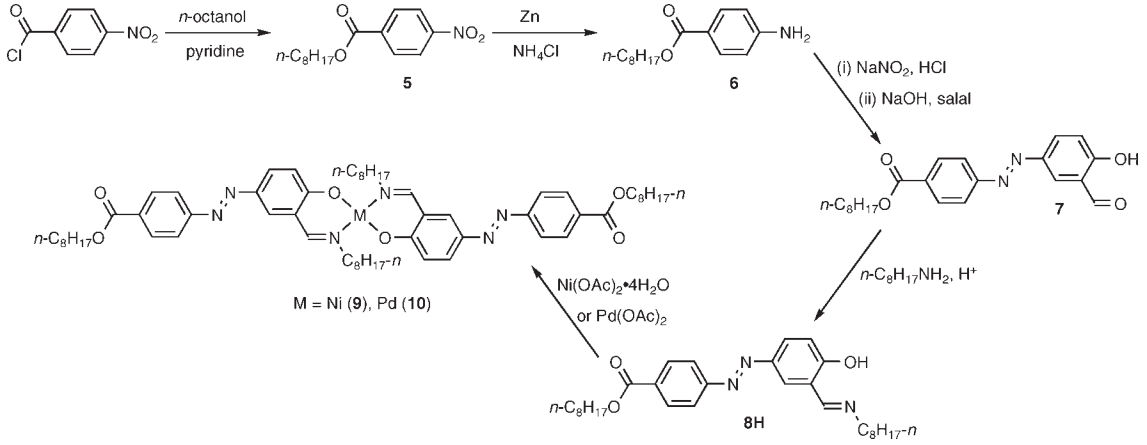

The precursor **1** was prepared via a diazonium coupling reaction with salicylaldehyde (salal) and isolated in a moderate yield. Schiff base condensations with the appropriate amines give the pro-ligands in yields ranging from 55% (**2aH**) to 90% (**2bH**).

The ethyl ester-functionalized complexes were obtained by reacting approximately 2 equiv of the appropriate pro-ligand with Ni^{II} or Pd^{II} acetate in ethanol under reflux. The reaction times were 2 h with $Ni^{II}(OAc)_2 \cdot 4H_2O$, but 24 h with $Pd^{II}(OAc)_2$, to allow for the decreased lability toward ligand substitutions of Pd^{II}. The products form as precipitates and were isolated in yields of 47−93% for M = Ni and 13−74% for M = Pd. However, not all of the Ni^{II} complexes were isolated. The complex of the *i*-propyl-substituted pro-ligand **2aH** was detected, but not isolated in pure form because of decomposition via ligand dissociation. The *t*-butyl-substituted pro-ligand **2bH** gave no trace of the desired complex from reactions in several different solvents, including attempts with added triethylamine base. These findings suggest that steric interactions of the bulkier Schiff base ligands about the Ni^{II} center may prevent the formation of stable complexes. The fact that this effect was observed only for nickel is consistent with the importance of steric effects since Ni^{II} is significantly smaller than Pd^{II}. The wide range of isolated yields for the Pd^{II} complexes may be due in part to solubility considerations. The low yield (13%) for complex **4b** was achieved after column chromatographic purification, while **4f** was isolated in a much higher yield and shows especially low solubility. The Pd^{II} complexes of the pro-ligands **2hH** and **2iH** were not prepared in view of the very poor solubility properties of their Ni^{II} counterparts.

To achieve more extended structures, an *n*-octyl ester analogue of **1** (**7**) was prepared via a diazonium coupling between 4-amino-*n*-octylbenzoate (**6**) and salal. Because **6** is not commercial, direct esterification of 4-aminobenzoic acid via the acid chloride was attempted, but this approach gave none of the desired product. Therefore, **6** was synthesized by the method shown in Scheme 2, using the activated precursor 4-nitrobenzoylchloride. 4-Nitro-*n*-octylbenzoate (**5**) is known,[28] but was prepared by using an adapted procedure that involves reacting *n*-octanol with 4-nitrobenzoylchloride in the presence of pyridine as a base.[29] This reaction proceeds almost quantitatively when using fresh 4-nitrobenzoylchloride, but hydrolysis of the acid chloride over time can limit the yield. **5** was reduced to **6** by using zinc and ammonium chloride in methanol.[30] The product contained about 5% of an impurity which could not be removed by column chromatography. This byproduct is likely to be a hydroxylamine intermediate, based on its ^{1}H NMR spectrum. Since the literature indicates that a hydroxylamine may not interfere with a diazonium coupling, such a reaction was

(28) See for example: (a) Armstrong, M. D.; Copenhaver, J. E. *J. Am. Chem. Soc.* **1943**, *65*, 2252. (b) Barry, J.; Bram, G.; Decodts, G.; Loupy, A.; Orange, C.; Petit, A.; Sansoulet, J. *Synthesis* **1985**, 40. (c) Loupy, A.; Pigeon, P.; Ramdani, M. *Tetrahedron* **1996**, *52*, 6705.

(29) Ohgiya, T.; Nakamura, K.; Nishiyama, S. *Bull. Chem. Soc. Jpn.* **2005**, *78*, 1549.

(30) Tsukinoki, T.; Tsuzuki, H. *Green Chem.* **2001**, *3*, 37.

Scheme 3. Syntheses of the New Biphenyl-Based Pro-Ligand **13H** and Its Ni/Pd Complexes

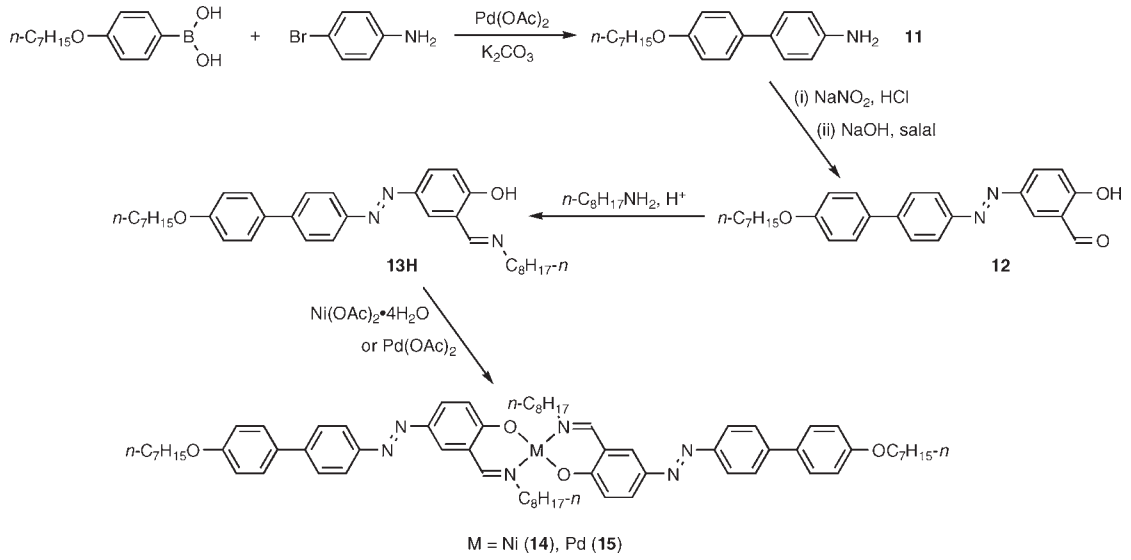

Scheme 4. Syntheses of the New Salen-Like Pro-Ligand $\mathbf{16H_2}$ and Its Ni/Pd Complexes

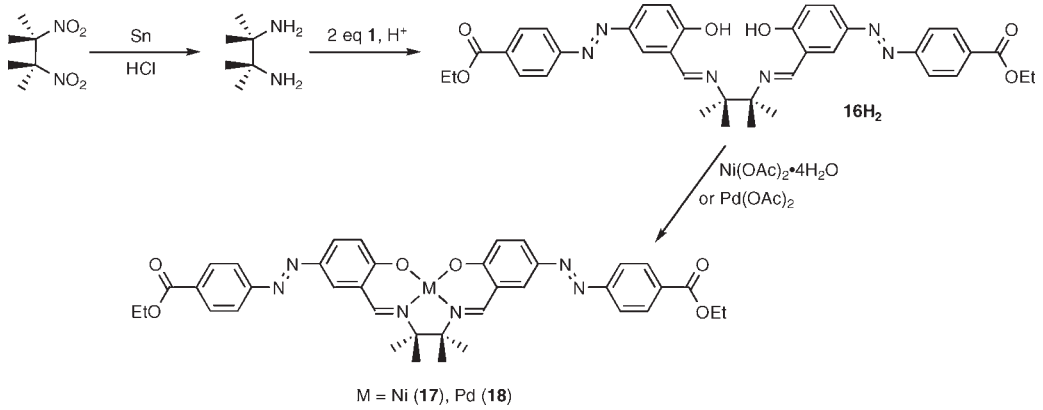

performed without further purification of **6**, producing **7** in a yield similar to that obtained for **1**. **7** was converted into its *n*-octyl Schiff base derivative **8H** which was then reacted with the metal acetates to produce complexes **9** and **10** (Scheme 2).

The biphenyl unit in the precursor compound **11** was formed via a Suzuki−Miyaura cross-coupling reaction (Scheme 3). **11** has been reported previously,[31] but was prepared via reduction of its nitro precursor. The required boronic acid was synthesized by slightly adapting a literature procedure which involves alkylation of 4-bromophenol followed by lithiation and reaction with tri-(*i*-propyl)-borate.[11] Coupling this boronic acid and 4-bromoaniline with $Pd^0(PPh_3)_4$ as a catalyst gives 4-(*n*-heptoxy)biphenyl as the major product after column chromatography. This undesired product is attributable to a side reaction involving exchange of Pd and P-bound aryl groups,[32] especially prevalent with electron-rich aryl halides,[33] but avoidable by using "ligand-less" Pd catalysts.[34] Hence, using $Pd^{II}(OAc)_2$ markedly improves the selectivity of the reaction and increases the yield of **11** by almost 3-fold. The latter was then diazotized and coupled with salal to afford **12**. The solubility of **12** is lower than that of its ester-substituted analogues, but improves on conversion into **13H**. Complexation of **13H** gives **14** and **15** (Scheme 3).

Complexes related to those described above but with the two azobenzenes cis-orientated are of interest. Previous studies have involved derivatives of *N*,*N*′-ethylenebis(salicylaldiminate) (salen) and closely related tetradentate species.[10a−c,e,i] We have carried out preliminary studies with pro-ligands prepared by condensing 2 equiv of **1** with 1,2-ethylenediamine and 1,2-phenylenediamine, but their Ni complexes are very poorly soluble in common organic solvents. However, the addition of methyl substituents increases solubility while not greatly expanding the molecular width, so we have also prepared the pro-ligand $\mathbf{16H_2}$ via condensation of **1** with 2,3-diamino-2,3-dimethylbutane (Scheme 4). The latter was prepared from commercial 2,3-dinitro-2,3-dimethylbutane via tin/HCl reduction according to a literature method.[12] $\mathbf{16H_2}$ leads to the complexes **17** and **18** which are more soluble than their unmethylated analogues.

(31) Kaharu, T.; Takahashi, S. *Mol. Cryst. Liq. Cryst.* **1994**, *257*, 35.
(32) (a) Kong, K.-C.; Cheng, C.-H. *J. Am. Chem. Soc.* **1991**, *113*, 6313. (b) O'Keefe, D. F.; Dannock, M. C.; Marcuccio, S. M. *Tetrahedron Lett.* **1992**, *33*, 6679.
(33) Goodson, F. E.; Wallow, T. I.; Novak, B. M. *J. Am. Chem. Soc.* **1997**, *119*, 12441.
(34) See for example: (a) Wallow, T. I.; Novak, B. M. *J. Org. Chem.* **1994**, *59*, 5034. (b) Moreno-Mañas, M.; Pajuelo, F.; Pleixats, R. *J. Org. Chem.* **1995**, *60*, 2396. (c) Badone, D.; Baroni, M.; Cardamone, R.; Ielmini, A.; Guzzi, U. *J. Org. Chem.* **1997**, *62*, 7170.

In addition to ^{1}H NMR spectroscopy (see below), the new compounds were characterized by satisfactory CHN elemental analyses, IR spectroscopy, and mass spectrometry. The Pd^{II} complexes **4a** and **4b** retain small amounts of dichloromethane of crystallization which was not removed by heating under vacuum. This residual solvent was detected in the ^{1}H NMR spectra by peaks at about 5.2 ppm integrating for the quantities indicated by the elemental analyses. For **4g** and **10**, the ^{1}H NMR spectra do not reveal any residual solvents, but the C analyses are lower than those expected, by about 3% for **4g** and 1% for **10**. Despite numerous repeat analyses, the data quoted are the best that could be obtained, and options for purification are especially limited for **4g** because of its very low solubility.

The imine group is expected to give a stretching band at about 1610−1630 cm^{-1}, and previous reports have noted low energy shifts of 10−30 cm^{-1} on metal complexation of such groups, implying decreased C=N bond order.[10d−h,35] Such shifts are consistent with π-back-bonding from the electron-rich metal to the imine unit. A similar situation applies to the new Ni^{II} complexes and also their Pd^{II} counterparts, excepting **4a** and **4c**. The ν(C=N) band energy is a little higher for the Pd^{II} complexes when compared with their Ni^{II} analogues, except for **4g** and **18** (the latter gives a broad band because of overlapped ν(C=N) and ν(C=C) absorptions). It is probably not appropriate to draw inferences concerning variations in bonding between the Ni^{II} and Pd^{II} complexes because IR absorptions can be influenced by intermolecular as well as intramolecular factors, especially in the solid-state. The pro-ligands and precursors give excellent mass spectra when using electrospray ionization. Most of the complexes do not give adequate spectra via electrospray, but MALDI gives good results, even with the insoluble phenyl derivatives, with excellent agreement between observed and predicted isotope patterns.

As noted above, solubility is an important consideration for potentially useful dichroic dyes. The pro-ligands **2aH**−**iH**, **8H**, **13H**, and **16H$_2$** show good solubility in common organic solvents; most are soluble in ethanol and all in chloroform. The complexes all precipitated out of ethanol during their syntheses, but are generally soluble in chloroform. However, the phenyl-substituted complexes **3g** and **4g** and the Ni^{II} complexes where R = OH (**3h**) or C_6H_4-4-CO_2Et (**3i**) show very low solubility and are only truly soluble in pyridine, attributable to axial ligation of this solvent to produce octahedrally coordinated complexes.[36] Such poor solubility hinders characterization and rules out any potential use as dichroic dyes. The presence of *N*-alkyl substituents hence appears to enhance the solubility of these complexes. However, the solubilities of the *n*-octyl ester-substituted complexes **9** and **10** are lower than those of their ethyl ester counterparts **3e** and **4e** (**9** and **10** precipitate from chloroform solutions on standing).

(35) Other examples: (a) Albert, J.; Granell, J.; Sales, J. *J. Organomet. Chem.* **1984**, *273*, 393. (b) Lee, M.; Yoo, Y. S.; Choi, M. G. *Macromolecules* **1999**, *32*, 2777.

(36) See for example: (a) Romano, V.; Maggio, F.; Pizzino, T. *J. Inorg. Nucl. Chem.* **1971**, *33*, 2611. (b) Warrier, K. G. K.; Pavithran, C.; Das, P. N. M.; Joseph, P. T. *Indian J. Chem.* **1978**, *16A*, 628. (c) Ma, Y.; Zhang, W.; Ou-Yang, Y.; Yoshimura, K.; Liao, D.-Z.; Jiang, Z.-H.; Yan, S.-P. *J. Mol. Struct.* **2007**, *833*, 98.

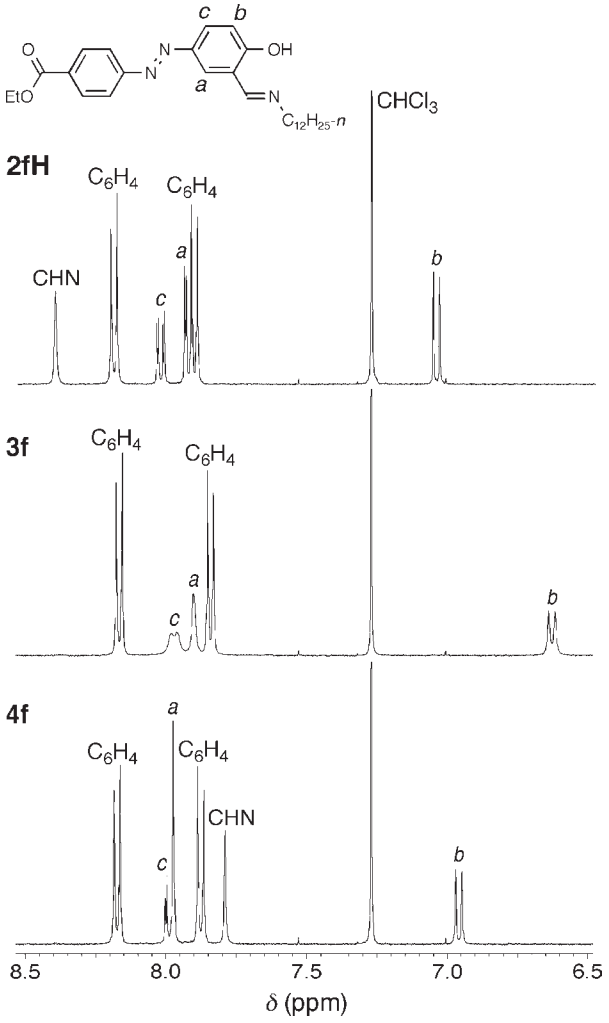

Figure 1. Aromatic regions of the ^{1}H NMR spectra of the pro-ligand **2fH** and its Ni^{II} (**3f**) and Pd^{II} (**4f**) complexes recorded at 400 MHz in $CDCl_3$ at 293 K.

^{1}H NMR Spectroscopy. Except for the poorly soluble complexes **3g**−**i** and **4g**, all of the new compounds give well-defined ^{1}H NMR spectra (in $CDCl_3$, except for **2hH** and **12**), consistent with their expected structures. Figure 1 shows representative spectra of the pro-ligand **2fH** and its Ni^{II} (**3f**) and Pd^{II} (**4f**) complexes, including the labeling scheme used for the C_6H_3 protons.

On conversion of the aldehydes **1**, **7**, and **12** into their respective Schiff bases **2aH**−**fH**, **2hH**, **8H**, **13H**, and **16H$_2$**, the methine proton singlet signal shifts upfield by about 1.6−1.8 ppm, reflecting the replacement of oxygen by the less electronegative nitrogen (note however that the spectra for **2hH** and **12** were recorded in $(CD_3)_2SO$). The corresponding shifts of about 1.25 ppm observed on moving from **1** to **2gH** or **2iH** are smaller than those for the other related imines because the electron-withdrawing phenyl substituents are deshielding while the alkyl groups are electron donors. The multiplet signals for the phenyl ring protons *a*, *b*, and *c* are readily assigned via their coupling constants; all of these also shift upfield on imine formation, but by only about 0.3 ppm or less. The OH singlet signal is found at 11.39 ppm for **1** and **7**. However, this signal is not observed for **12** in $(CD_3)_2SO$, or for many of the Schiff base pro-ligands, but gives a broad resonance

in the region of about 14−14.8 ppm for **2eH**−**gH**, **13H** and **16H$_2$**. Sharper phenoxy OH singlets are observed at 13.60 ppm for **2iH** and at 11.53 ppm for **2hH**; in the latter, the singlet at slightly higher field (11.03 ppm) is likely to be attributable to the hydroxyl group attached to the more shielding imine unit. The OH signal is readily distinguished from the aldehyde signal in **1** and **7** by its slightly broadened appearance and higher chemical shift.

On deprotonation of the alcohols **2cH**−**fH**, **8H,** and **13H** and complexation to Ni^{II}, peaks corresponding to protons close to the metal center become broadened. The imine signal is the most affected, with the triplet signal for the CH_2 protons adjacent to the imine group and the signals for protons *a*−*c* also showing some broadening. These effects are attributable to a degree of paramagnetic character due to slight distortions toward a tetrahedral coordination geometry. Previous studies with related complexes provide ample precedents for such behavior.[37] Notably, the *i*-propyl-substituted complex derived from **2aH** which decomposed readily (see above) showed a set of sharp NMR signals corresponding to the ethyl group and the phenylene ring protons, with several broad signals. These observations indicate a more severe distortion toward a tetrahedral geometry in solution, attributable to steric considerations.

Significant peak shifts are also observed on complexation of the pro-ligands to Ni^{II}. The imine proton signal shifts downfield by about 0.5−1.1 ppm, and the doublet signal for proton *b* shifts upfield by about 0.4 ppm. The NCH_2 signals are also shifted downfield by up to 0.4 ppm. The doublet of doublets for proton *c* shifts upfield, but by only about 0.1 ppm or less, while even smaller shifts are detected for the doublet for proton *a*. These shifts are probably associated significantly with the paramagnetism discussed above. Notably, for the salen-like pro-ligand **16H$_2$**, a quite different pattern of shifts is observed on moving to complex **17**. An absence of signal broadening implies a perfectly square planar geometry in solution imposed by the rigidity of the tetradentate ligand. The *a* and *c* proton signals still shift slightly upfield, but the *b* proton signal shifts *downfield* by 0.09 ppm, and the imine proton signal moves *upfield* by 0.8 ppm. Note however that slight distortion is nonetheless observed in the solid-state structure of **17** (see below).

The ^{1}H NMR spectra of the Pd^{II} complexes show no broadening, consistent with their expected perfectly square planar structures. Pd^{II} complexation of the pro-ligands **2aH**, **2cH**−**fH**, **8H,** and **13H** shifts the imine proton signal upfield by about 0.6 ppm (Figure 1), showing increased shielding. Only slight shifts are observed for the C_6H_3 signals; the *a* proton signal shifts downfield by 0.04−0.08 ppm, while the *b* and *c* proton signals shift upfield. Notably, the Pd^{II} complexation-induced shifts of the signals for the *t*-butyl derivative **2bH** differ greatly from those observed for the other closely related species. The imine proton signal shows a larger upfield shift of 0.87 ppm in **4b**, while the signals for protons *a*−*c* all shift downfield slightly. On Pd^{II} complexation of **16H$_2$**, the imine proton signal shifts upfield by 0.51 ppm, while the signals for protons *a*, *b*, and *c* all shift downfield, by 0.08, 0.23, and 0.07 ppm, respectively.

The upfield shifting of the imine signals for all of the Pd^{II} complexes and the Ni^{II} complex **17** is evidence for π-back-bonding from the metal centers. The large deshielding effects evident for the imine signal in all of the Ni^{II} bis-chelates appear to contradict the corresponding shielding observed in their Pd^{II} analogues. However, the likely presence of paramagnetic shifts precludes conclusions regarding π-back-bonding in the Ni^{II} bis-chelates. Without complicating paramagnetism, comparison of the shifts observed for the imine signals of complexes **17** and **18** is valid. The respective peak positions of 7.67 and 7.96 ppm suggest that π-back-bonding is stronger in the Ni^{II} complex than its Pd^{II} counterpart, since the upfield shift of about 0.3 ppm on moving from **18** to **17** indicates greater shielding.

Finally, it is worth noting that the ^{1}H NMR spectra of both the new pro-ligands and complexes show some evidence for trans-to-cis photoisomerization of the azobenzene units. The observed minor signals shifted to higher field with respect to the main peaks are characteristic of *cis*-azobenzenes,[38] and these are present in levels as high as about 16%. When the samples are placed in amberized NMR tubes which block light of 300−800 nm, the minor signals disappear, indicating thermal relaxation back to the trans isomers.

Electronic Spectroscopy Studies. The UV−vis absorption spectra of the new pro-ligands and complexes have been measured in dichloromethane, and the results are shown in Table 2. Representative spectra of **2cH**, **3c**, **4c** and **13H**, **14**, and **15** are shown in Figure 2.

The pro-ligands show intense absorptions with λ_{max} in the range 353−379 nm, characteristic of the $\pi \rightarrow \pi^*$ intramolecular charge-transfer (ICT) transitions of azobenzene. In each case, a pronounced shoulder on the low energy side of the ICT absorption is attributable to the $n \rightarrow \pi^*$ transition which appears at about 450 nm for *trans*-azobenzene.[39] Each compound also displays a second, less intense band to higher energy, with λ_{max} in the range 246−278 nm.

On complexation, λ_{max} of the dominant absorption band increases (Figure 2), indicating that the energy gap between the highest occupied molecular orbital (HOMO) and the lowest unoccupied molecular orbital (LUMO) decreases. It is likely that the ICT process acquires some degree of metal-to-ligand charge-transfer (MLCT) character, with the HOMO energy being raised by deprotonation and complexation of the hydroxyl group. The red shifts are almost constant at about 0.5 eV on moving from the pro-ligands **2cH**−**2fH**, **8H** and **16H$_2$** to their Ni^{II} complexes, but a smaller shift of 0.3 eV is observed for the biphenyl derivatives **13H** and **14**. Generally smaller relative red shifts occur on coordination of the pro-ligands to Pd^{II}; about 0.4 eV for **2aH**, **2cH**−**2eH**, **8H**, and **16H$_2$**, but 0.25 eV for **2bH** and **13H**. The main absorptions of the Pd^{II} complexes are hence blue-shifted (by 0.05−0.13 eV) with respect to those of their Ni^{II} analogues (Figure 2). These blue shifts are consistent with greater stabilization of

(37) See for example: (a) Sacconi, L.; Paoletti, P.; Ciampolini, M. *J. Am. Chem. Soc.* **1963**, *85*, 411. (b) Holm, R. H.; Swaminathan, K. *Inorg. Chem.* **1963**, *2*, 181. (c) Sacconi, L.; Ciampolini, M. *J. Am. Chem. Soc.* **1963**, *85*, 1750. (d) Sacconi, L.; Ciampolini, M.; Nardi, N. *J. Am. Chem. Soc.* **1964**, *86*, 819.

(38) Tait, K. M.; Parkinson, J. A.; Bates, S. P.; Ebenezer, W. J.; Jones, A. C. *J. Photochem. Photobiol. A* **2003**, *154*, 179.

(39) Haberfield, P.; Lux, M. S.; Rosen, D. *J. Am. Chem. Soc.* **1977**, *99*, 6828.

Table 2. UV−vis Absorption Data for the New Pro-Ligands and Their Ni^{II}/Pd^{II} Complexes in Dichloromethane[a]

pro-ligand	λ_{max}, nm (ε, 10^3 M^{-1} cm^{-1}) /E_{max}, eV	Ni^{II} complex	λ_{max}, nm (ε, 10^3 M^{-1} cm^{-1}) /E_{max}, eV	Pd^{II} complex	λ_{max}, nm (ε, 10^3 M^{-1} cm^{-1}) /E_{max}, eV
2aH	370 (21.3)/3.35 277 (14.7)/4.48			**4a**	418 (52.5)/2.97 278 (27.9)/4.46
2bH	378 (20.9)/3.28 276 (14.0)/4.49			**4b**	408 (43.4)/3.04 259 (40.2)/4.79
2cH	370 (21.0)/3.35 274 (15.6)/4.53	**3c**	433 (47.3)/2.86 344 (22.5)/3.60 269 (33.3)/4.61	**4c**	418 (74.5)/2.97 280 (36.9)/4.43
2dH	371 (22.2)/3.34 277 (15.4)/4.48	**3d**	434 (59.3)/2.86 339 (26.6)/3.66 269 (38.7)/4.61	**4d**	419 (69.3)/2.96 280 (34.3)/4.43
2eH	372 (23.7)/3.33 278 (14.9)/4.46	**3e**	429 (63.2)/2.89 347 (30.1)/3.57 270 (47.8)/4.59	**4e**	418 (61.9)/2.97 280 (35.5)/4.43
2fH	371 (27.7)/3.34 277 (17.1)/4.48	**3f**	433 (63.9)/2.86 338 (29.0)/3.67 269 (42.1)/4.61	**4f**	418 (67.9)/2.97 280 (34.3)/4.43
2gH	353 (34.0)/3.51 266 (17.1)/4.66		*b*		*b*
8H	371 (23.9)/3.34 276 (15.2)/4.49	**9**	434 (56.3)/2.86 339 (25.7)/3.66 269 (37.3)/4.61	**10**	418 (73.7)/2.97 279 (36.1)/4.44
13H	379 (36.4)/3.27 246 (22.6)/5.04	**14**	418 (66.3)/2.97 252 (41.4)/4.92	**15**	411 (79.8)/3.02 241 (50.9)/5.15
$16H_2$	370 (51.9)/3.35 276 (34.0)/4.49	**17**	433 (51.9)/2.86 257 (44.7)/4.82	**18**	418 (71.1)/2.97 271 (35.2)/4.58

[a] Solutions about 4×10^{-6}−6×10^{-5} M. The ε values are the averages from measurements made at four different concentrations (with ε showing no significant concentration dependence). [b] Not measured because of insufficient solubility.

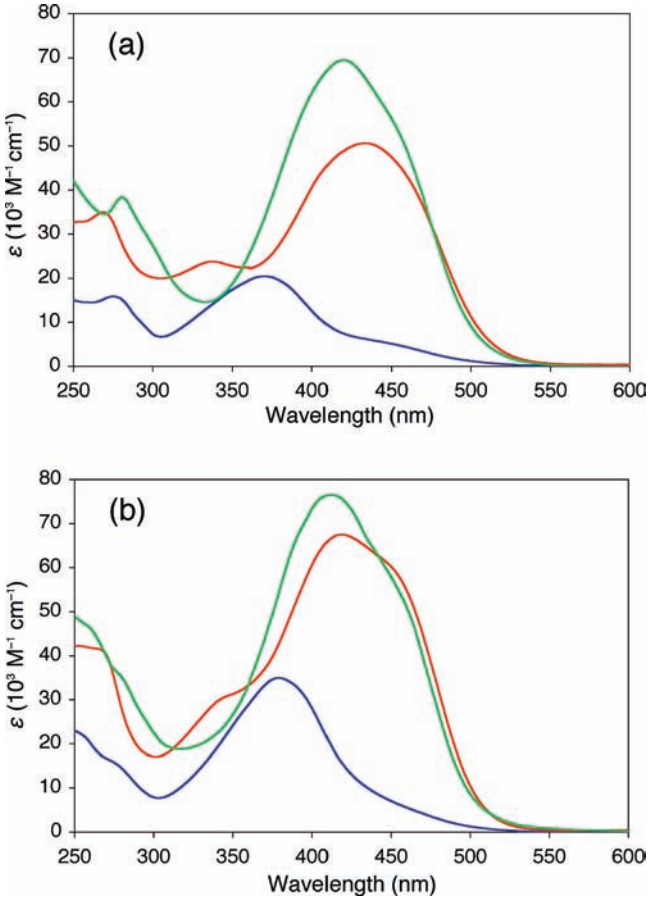

Figure 2. UV−vis absorption spectra in dichloromethane at 293 K: (a) the pro-ligand **2cH** (blue), its Ni^{II} complex **3c** (red), and its Pd^{II} complex **4c** (green); (b) the pro-ligand **13H** (blue), its Ni^{II} complex **14** (red) and its Pd^{II} complex **15** (green).

the HOMO for Pd^{II} when compared with Ni^{II}, because of the increase in effective nuclear charge when moving from a first to second row transition metal.[40] In all cases except for **$16H_2$**, the ε values increase about 2−3-fold on complexation, since two azobenzene chromophores are combined into one molecule. For 5 out of 7 comparable pairs, the band intensities are also considerably larger for the Pd^{II} complexes than for their Ni^{II} analogues. For **$16H_2$**, ε remains unchanged on complexation to Ni^{II} (**17**), but increases by about 40% on moving to the Pd^{II} complex **18**. Most of the Ni^{II} complexes also display a shoulder on the high energy side of their ICT band, but this is not the case for their Pd^{II} counterparts. The ICT bands of the biphenyl-containing complexes **14** and **15** are slightly blue-shifted when compared with those of the other related species because of the replacement of an electron-accepting ester with an 4-(*n*-heptoxy)phenyl electron donor.

Crystallographic Studies. Single crystal X-ray structures have been obtained for the pro-ligands **2eH** and **2gH** and the complexes **3e**, **4e**, **14**, **15**, and **17**. Representations of the molecular structures are shown in Figures 3−9, and selected geometric parameters in Table 3.

The structure of **2eH** (Figure 3) shows a hydrogen bond between the hydroxyl proton and the nearby imine nitrogen with a N···H distance of 1.84 Å. The two phenyl rings of the azobenzene unit are almost coplanar, with a dihedral angle of 5.5(1)°. In the closely related **2gH** (Figure 4), the hydrogen-bond distance is 1.86 Å, and the dihedral angle within the azobenzene group is 7.4(1)°. A much larger twist of 41.3(1)° is observed between the *N*-phenyl substituent and the nearby phenolic ring.

(40) (a) Kirgan, R. A.; Rillema, D. P. *J. Phys. Chem. A* **2007**, *111*, 13157. (b) Shimazaki, Y.; Stack, T. D. P.; Storr, T. *Inorg. Chem.* **2009**, *48*, 8383.

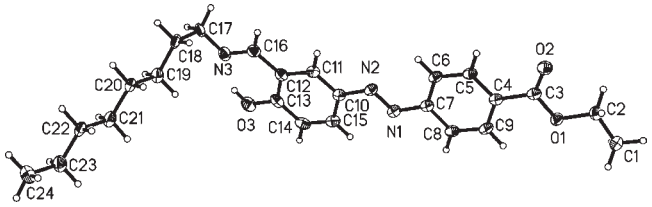

Figure 3. Representation of the molecular structure of **2eH**, with the disorder in the *n*-octyl chain removed (50% probability ellipsoids).

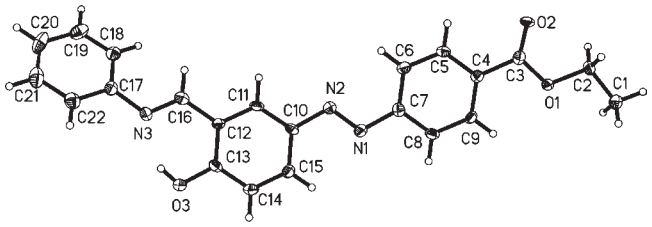

Figure 4. Representation of the molecular structure of **2gH** (50% probability ellipsoids).

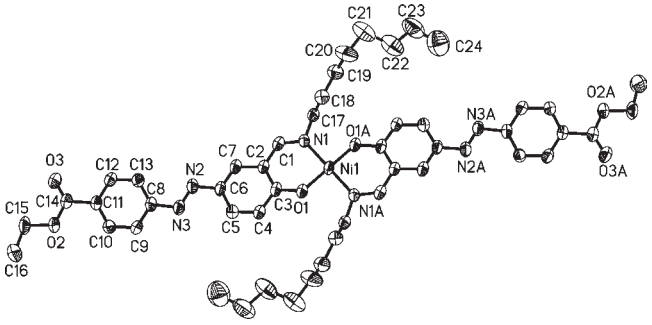

Figure 5. Representation of the molecular structure of **3e**, with the disorder in the *n*-octyl chains removed and H atoms omitted for clarity (50% probability ellipsoids).

The structure of complex **3e** (Figure 5) is in most respects reminiscent of that reported for the analogous complex having instead *n*-pentyl groups on the imine N atoms and *n*-butyl substituents in place of the ester units.[10d] Although many similar structures of molecules containing the central N_2O_2-coordinated Ni^{II} core have been reported, there appear to be no others with azobenzene substituents. The mostly noteworthy point relating to **3e** is that the coordination geometry around the Ni^{II} ion is strictly square planar. It is hence apparent that the slight distortions toward tetrahedral geometry inferred in solution from ^1H NMR spectra (see above) are absent in the solid state. Nevertheless, it is quite conceivable that some departure from planarity may occur when such complexes are dissolved in a LC medium. Furthermore, the previously reported related structure does show a significant distortion, with a dihedral angle of 13.2° between the two fully planar six-membered chelate rings.[10d]

As expected, the two chelating ligands in **3e** adopt a trans arrangement with respect to the planar core, preventing steric clashes between the *n*-octyl chains. When compared with the pro-ligand **2eH**, **3e** shows a much larger dihedral angle of 24.2(1)° between the two rings of the azobenzene units. The C=N distance in the imine group is significantly longer in **3e** when compared with **2eH**, while the phenolic C−O and the C−C distance between the imine unit and phenyl ring both shorten somewhat on Ni^{II} complexation

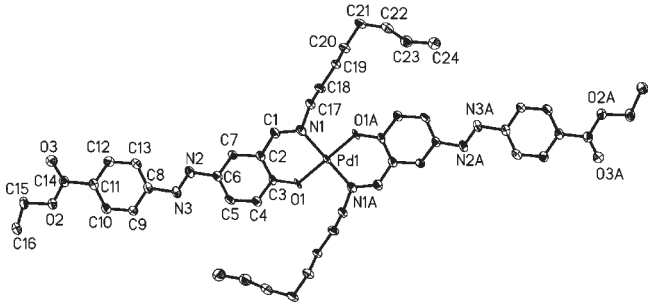

Figure 6. Representation of the molecular structure of **4e**, with the H atoms omitted for clarity (50% probability ellipsoids).

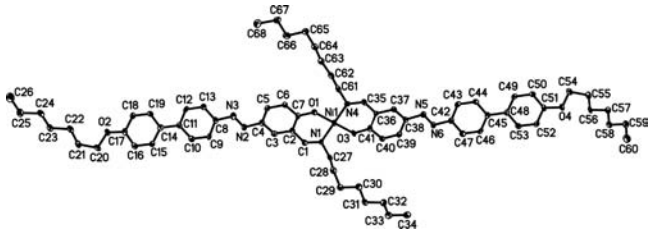

Figure 7. Representation of the molecular structure of **14**, with the H atoms omitted for clarity (50% probability ellipsoids).

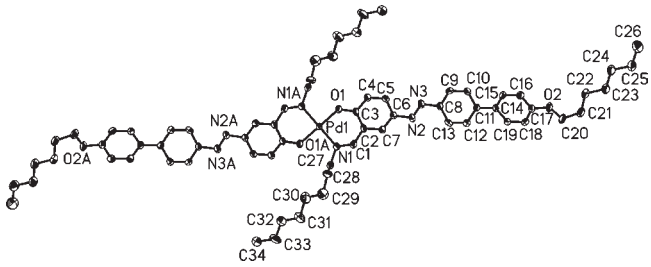

Figure 8. Representation of the molecular structure of **15**, with the disorder in the *n*-octyl chains removed and H atoms omitted for clarity (50% probability ellipsoids).

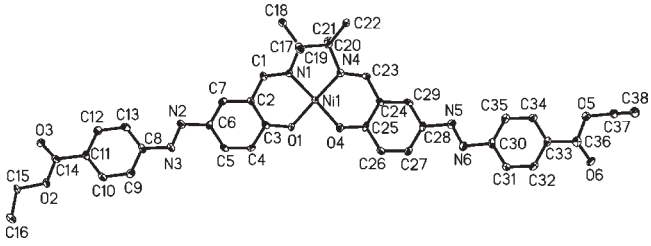

Figure 9. Representation of the molecular structure of **17**, with the H atoms omitted for clarity (50% probability ellipsoids).

(Table 3). The phenyl C−C distance that is also part of the six-membered chelate ring does not change significantly on moving from **2eH** to **3e**.

The structure of the analogous Pd^{II} complex **4e** (Figure 6) also shows a strictly square planar geometry, as expected. Once again, various related structures have been reported (although not as many as for Ni^{II}, and lacking azobenzene groups).[41] In **4e**, the azobenzene dihedral angle is less than

(41) See for example: (a) Lanfredi, A. M. M.; Ugozzoli, F.; Ghedini, M.; Licoccia, S. *Acta Crystallogr., Sect. C* **1985**, *41*, 192. (b) Ghedini, M.; Pellegrino, C.; Armentano, S.; de Munno, G.; Bruno, G. *Inorg. Chim. Acta* **1986**, *122*, 193. (c) Lai, Y.-C.; Chen, H.-Y.; Hung, W.-C.; Lin, C.-C.; Hong, F.-E. *Tetrahedron* **2005**, *61*, 9484.

Table 3. Selected Interatomic Distances (Å) and Angles (deg) for the Pro-Ligands **2eH** and **2gH** and for the Complexes **3e**, **4e**, **14**, **15**, and **17**

	2eH	2gH	3e	4e	14	15	17
C═N	1.279(2)	1.280(3)	1.304(4)	1.353(12)	1.291(6), 1.286(6)	1.290(5)	1.293(5), 1.294(5)
C(im)[a]−C(Ph)	1.454(2)	1.459(4)	1.428(4)	1.446(13)	1.418(7), 1.431(7)	1.436(6)	1.438(6), 1.431(6)
C(Ph)−C(Ph)[b]	1.407(2)	1.404(4)	1.396(5)	1.425(14)	1.431(7), 1.422(7)	1.421(6)	1.412(6), 1.420(6)
C(Ph)−O	1.349(2)	1.347(3)	1.317(4)	1.332(11)	1.310(6), 1.309(6)	1.309(5)	1.302(5), 1.300(5)
M−O			1.833(3)	2.008(6)	1.826(3), 1.832(3)	1.978(3)	1.844(3), 1.847(3)
M−N			1.917(3)	2.027(8)	1.932(4), 1.931(4)	2.025(4)	1.853(3), 1.846(3)
C−N−C[c]	119.4(6)	120.1(3)	114.5(3)	114.4(8)	114.0(4), 113.5(4)	116.1(4)	120.0(4), 120.0(4)
N−C−C[d]	121.90(17)	121.6(3)	127.0(3)	126.9(10)	127.9(5), 127.6(5)	129.2(5)	125.2(4), 125.6(4)
N−M−O[e]			93.04(16)	91.4(3)	92.80(17), 92.32(17)	92.16(14)	94.98(14), 95.13(14)
N−M−O			86.96(16)	88.6(3)	87.18(18), 87.72(17)	87.84(14)	173.46(15), 175.14(14)
N−M−N							86.75(16)
O−M−O							83.65(13)

[a] im = imine. [b] For the bond within the chelating unit. [c] Angle subtended at the imine N atom. [d] Angle subtended at the imine C atom. [e] Within the six-membered chelate rings.

half of that in **3e** (11.4(3)°), although this difference is likely due to crystal packing forces rather than intramolecular electronic effects. As expected, the metal−ligand distances in **4e** are somewhat larger than those in **3e**. On moving from this Ni^{II} complex to its Pd^{II} analogue, the M−O distance increases by about 0.18 Å, while the corresponding increase for the M−N distance is about 0.11 Å. The N−M−O chelating angle is slightly larger in **3e** when compared with **4e**, while the imine C═N distance is slightly longer in **4e** than in **3e** (Table 3).

The structure of the Ni^{II} complex **14** (Figure 7) resembles that of **3e**, with a fully square planar geometry and indistinguishable bond distances and angles around the metal center. The length of the molecule from alkoxy oxygen to its symmetry-related partner is 34.9 Å, and the structure is quite twisted with respective dihedral angles of 28.2(2)/31.2(2) and 17.6(2)/22.3(2)° within the biphenyl and azobenzene units. Except for some disorder at the ends of the alkyl chains, the analogous Pd^{II} complex **15** (Figure 8) is essentially isostructural with **14**, with corresponding dihedral angles of 30.4(2) and 17.8(1)°. Again, the bond distances and angles around the metal center are very similar for **15** and **4e**. On moving from **14** to **15**, the average M−O distance increases by about 0.15 Å, while the corresponding increase for the M−N distance is about 0.09 Å. The imine C═N distances in **14** and **15** are effectively identical, so it is not appropriate to propose electronic changes as causing the apparent small difference in these distances observed between **4e** and **3e** (see above). For each of **3e**, **4e**, **14**, and **15**, the M−N distances are larger than the M−O distances, but the differences are noticeably greater for the Ni^{II} complexes (ca. 0.08 and 0.10 Å for **3e** and **14**, respectively) than for their Pd^{II} counterparts (ca. 0.02 and 0.05 Å for **4e** and **15**, respectively).

The structure of the Ni^{II} complex **17** (Figure 9) resembles those of related species containing a similar chelating motif,[42] although no structures of similar azobenzene-substituted complexes have been reported to our knowledge. The inevitable cis disposition of the N atoms in **17** does not greatly influence the Ni−O distances, but the Ni−N distances are shortened by about 0.07−0.08 Å when compared with those in **3e** and **14**. This difference is probably attributable to the presence of a linkage between the N atoms, and means that the Ni−O and Ni−N distances in **17** are not significantly different. The O−M−N angle in **17** is slightly larger (by ca. 2°) when compared with those in **3e** and **14**. In contrast to **3e** and **14**, but as for the more closely related structures in the literature,[42] **17** shows a sight distortion away from perfect square planar coordination geometry, with an angle of 7.54(0.12)° between the planes defined by O1−Ni1−N1 and O4−Ni1−N4. The molecule is distinctly bowed when viewed sideways, with one azobenzene unit only slightly twisted (dihedral angle = 9.35(0.12)°), but the other much more so (dihedral angle = 30.13(0.14)°). The torsion angle of the ethylene bridging unit (N1−C17−C20−N4) is 43.3(4)°.

Table 4. Dichroic Ratios Measured in LC Hosts

compound	ZLI-2293	ZLI-1132	K15
2aH	5.2		3.6
2bH	5.4		3.2
2cH	5.4		3.7
2dH	5.5		3.3
2eH	5.0		3.4
2fH	6.0		3.9
8H	5.3		2.8
13H	8.4	8.1	6.3
14	12.1	10.6	
15	5.8	5.8	
16H$_2$	5.5		3.7
17	9.7		7.0
18	5.4		3.7

Dichroic Ratio Measurements. The pro-ligands are highly soluble in a range of LCs and their *DR*s measured in both ZLI-2293[43] and K15 (4-pentyl-4′-cyanobiphenyl) are shown in Table 4. It should be noted that a lower wavelength limit of 380 nm is imposed by the spectrometer used, so the *DR*s quoted are not necessarily calculated at the absorption maximum. The values in K15 are lower than those in ZLI-2293 since the lower clearing temperature of the LC corresponds to a lower *S* at room temperature. A correlation between the *S* of a host LC and *DR* values of dissolved dyes is established.[5,44] The

(42) (a) de C. T. Carrondo, M. A. A. F.; de Castro, B.; Coelho, A. M.; Domingues, D.; Freire, C.; Morais, J. *Inorg. Chim. Acta* **1993**, *205*, 157. (b) Fritzsche, S.; Lönnecke, P.; Höcher, T.; Hey-Hawkins, E. *Z. Anorg. Allg. Chem.* **2006**, *632*, 2256.

(43) The precise compositions and chemical identities of the commercial LC mixtures ZLI-1132 and ZLI-2293 are unknown to us. However, comparisons of their ^{1}H NMR spectra obtained in $CDCl_3$ with that of the reference compound 4-(*trans*-4-*n*-pentylcyclohexyl)bromobenzene indicate that both of these substances contain primarily 4,4′-disubstituted cyclohexylbenzene derivatives with long alkyl chain(s).

(44) Ichinose, H.; Sato, H.; Naemura, S. *Mol. Cryst. Liq. Cryst.* **2004**, *409*, 401.

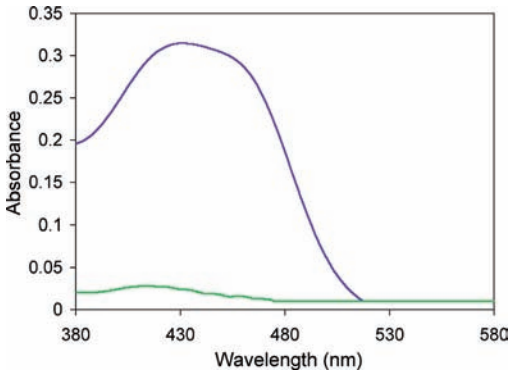

Figure 10. Absorption profiles measured parallel (purple) and perpendicular (green) to the LC director for the Ni^{II} complex **14** in ZLI-1132.

*DR*s for all of the pro-ligands, except **13H**, are the same within experimental error. Notably, neither the presence of a longer terminal alkyl chain (in **8H**) nor the connection of two chromophores via an ethylene bridge (in **16H$_2$**) improves the dichroism when compared with the bidentate ethyl ester-substituted pro-ligands. Different R groups (Scheme 1) also do not affect the *DR* value. The biphenyl-based **13H** shows a significantly higher *DR*, probably as a result of better ordering within the LC because of its mesogenic subunit.

Unfortunately, most of the complexes show poor solubility in the widely used single-component LC K15 and insufficient absorption precludes meaningful measurements. Their solubility in commercial LC mixtures (ZLI-2293, etc.) is far superior to that in K15, although in most cases a 5 μm path length does not provide sufficient absorption intensity.

The biphenyl-based complexes **14** and **15** are the most soluble of the bis-bidentate species. Using two adjacent cells to give sufficient absorption, the *DR*s for these compounds determined in ZLI-2293 and ZLI-1132 are shown in Table 4. A representative absorption spectrum is shown in Figure 10. The Ni^{II} complex **14** has a significantly higher *DR* when compared with its pro-ligand **13H** in ZLI-2293. However, in ZLI-1132, the observed increase may not be significant. The increases in *DR* are certainly less than 2-fold, although the length of the dye is at least doubled. Several factors may prevent a doubling of the *DR*. An accompanying increase in the width of the dye because of the staggered nature of the coordination sphere, implies that the length-to-diameter ratio (l/d) is less than double that of the pro-ligand.[5c] Nevertheless, the *DR* of **14** is sufficiently high for potential electronic device applications. Interestingly, the *DR*s of the Pd^{II} complex **15** are smaller than those of the pro-ligand, despite being essentially isostructural with **14**. The origin of these decreases is unclear, although possible explanations include dimerization via Pd−Pd interactions. Such effects have been invoked to explain an absence of LC behavior for Pd^{II} bis-dithiolene complexes when compared with their Ni^{II} (and also Pt^{II}) analogues,[45] but do seem rather unlikely here, given the low concentrations involved. More generally, intermolecular interactions between dye and LC play an important role in influencing *DR*s, and these may be affected by the differing sizes of the metal ions and charge distributions in the complexes.

(45) Mueller-Westerhoff, U. T.; Nazzal, A.; Cox, R. J.; Giroud, A. M. *Mol. Cryst. Liq. Cryst.* **1980**, *56*, 249.

The complexes **17** and **18** are more soluble than the bis-bidentate species, so were studied in K15 as well as ZLI-2293; the results are presented in Table 4. Once again, an increase in *DR* is observed on complexation of the pro-ligand to Ni^{II} (in **17**). The flexibly linked chromophores in **16H$_2$** become one long, rigid dye on complexation. The *DR* increases in this case are apparently larger than those for the biphenyl complexes, being almost 2-fold in K15. This more pronounced effect of complexation may be because the l/d ratio increases more dramatically when compared with the bis-bidentate compounds. Notably, the *DR*s of the Pd^{II} complex **18** are essentially the same as for **16H$_2$**. The factor(s) causing a decline in dichroism on moving from Ni to Pd is/are apparently less effective in the tetradentate system.

Theoretical Studies. To rationalize the electronic structures and optical properties of the representative pro-ligand **2eH** and its Ni^{II} complex **3e**, ZINDO_S calculations were carried out by using Gaussian 03,[21] with ORCA[22] for structural optimization. The UV−vis spectra were simulated (GaussSum)[27] by using both the optimized and the X-ray crystallographic (see above) geometries. Using the latter structures gives reasonable agreement with the experimental data for **2eH**, but a lesser degree of correlation is found for the complex (Supporting Information, Figure S1). The predicted transition energies are presented in Supporting Information, Table S1, and the principal orbitals involved in the ICT transitions are shown in Supporting Information, Figures S2−S5.

Since time-dependent density functional theory (TD-DFT) has become the preferred computational approach recently, such calculations were performed on model systems by using Gaussian 03.[21] The models were obtained from the crystal structures of **2eH** and **3e** by replacing the octyl and ethyl chains with methyl groups (the alkyl chains are not expected to affect signficantly the electronic structures). Geometries optimized at the BP86/Def2-SVP level[23,24] were used in TD-DFT calculations of the electronic spectra (Figure 11 and Supporting Information, Figure S6), with the B3LYP[25] and MPW1PW91[26] functionals. It is known that B3LYP can give poor predictions of ICT transitions and MPW1PW91 is apparently better at describing such processes. The predicted transition energies are shown in Table 5, and the principal orbitals involved in the main transitions are depicted in Figures 12 and 13.

When comparing the TD-DFT predictions with the experimental absorption spectra for **2eH** and **3e** (Figures 11 and Supporting Information, Figure S6), both functionals give quite similar results and reproduce the qualitative details well, with B3LYP generally giving transition energies slightly lower than MPW1PW91 (Table 5). For the pro-ligand, the ICT energy is slightly better predicted by using MPW1PW91, while B3LYP gives a closer match with the experimental profile for the nickel complex. The relative superiority of TD-DFT over the ZINDO_S method is most readily apparent for the complex, with the latter predicting a substantial increase of about 0.3 eV in the ICT E_{max} (Figures 11b, Supporting Information, Figures S1b and S6b).

For the methylated pro-ligand model, BP86/Def2-SVP geometry optimization yields an almost completely planar structure that resembles that observed for **2eH** via X-ray crystallography (see above). Both the ZINDO_S calculations with the X-ray structure and the TD-DFT studies confirm the $\pi \rightarrow \pi^*$ nature of the major excitation

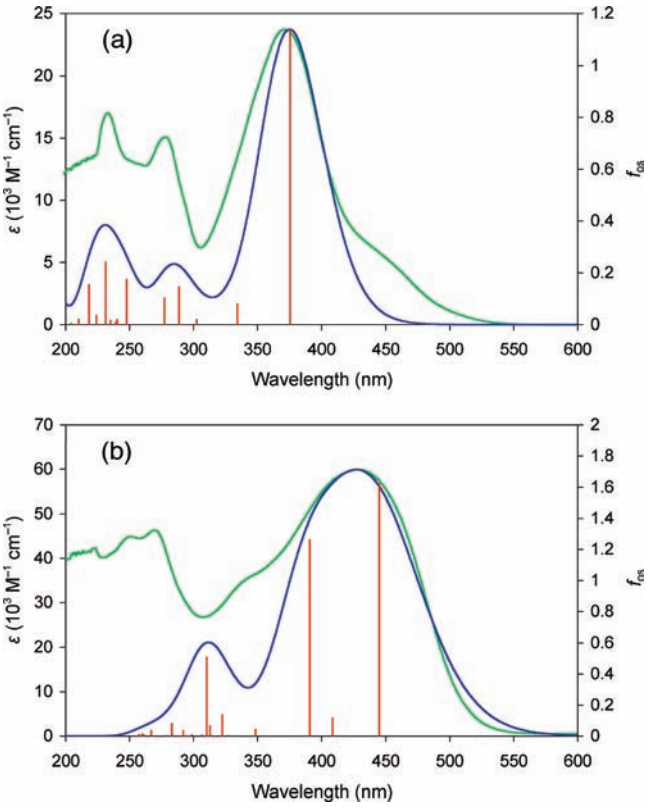

Figure 11. TD-DFT-calculated (blue) UV−vis spectra of (a) the pro-ligand model system (MPW1PW91) and (b) the Ni^{II} complex model system (B3LYP); and experimental (green) UV−vis spectra of (a) **2eH** and (b) **3e**. The ε-axes refer to the experimental data only and the vertical axes of the calculated data are scaled to match the main experimental absorptions. The oscillator strength axes refer to the individual calculated transitions (red).

(Figure 12 and Supporting Information, Figure S7), showing that the π-bonding and antibonding orbitals involved span both rings, their substituents and the azo unit. This picture is consistent with previous studies on azobenzenes.[46] The ZINDO_S calculations also predict a very weak excitation to low energy of the ICT band (Supporting Information, Table S1), possibly attributable to an n → π^* transition. Interestingly, optimization of the molecular structure using the ZNDDO_2 procedure, as implemented in ORCA, results in a large dihedral angle (83.7°) between the two rings which contrasts strongly with the crystal structure (see above). ZINDO_S calculations using this highly twisted geometry produce a similar electronic picture, but the ester-substituted phenyl ring no longer contributes to the frontier orbitals (Supporting Information, Figure S4).

BP86/Def2-SVP geometry optimization of the methylated model for Ni complex **3e** again produces an almost perfectly planar structure. TD-DFT calculations with B3LYP show that two transitions lead to the broad ICT profile observed experimentally (Figure 11b). The MPW1PW91 functional affords a similar picture, but with slightly higher transition energies and a less equal weighting (Supporting Information, Figure S6). When using either functional, the lowest energy intense ICT transition is HOMO → LUMO in nature, with the next lowest energy transition being HOMO−1 → LUMO+1 (Figure 13 and Supporting Information,

(46) See for example: (a) Forber, C. L.; Kelusky, E. C.; Bunce, N. J.; Zerner, M. C. *J. Am. Chem. Soc.* **1985**, *107*, 5884. (b) Bhat, K. L.; Trachtman, M.; Bock, C. W. *Dyes Pigments* **2001**, *48*, 197. (c) Zaleśny, R.; Matczyszyn, K.; Kaczmarek, A.; Bartkowiak, W.; Cysewski, P. *J. Mol. Model.* **2007**, *13*, 785.

Table 5. Data from TD-DFT Calculations Based on BP86/Def2-SVP Geometries of the Pro-ligand and Ni^{II} Complex Models

functional	ΔE (eV)	f_{os}	major contributions	μ_{12} (D)
		Pro-Ligand		
B3LYP	3.21	1.10	HOMO → LUMO	9.52
	4.13	0.12	HOMO−3 → LUMO	2.76
			HOMO−4 → LUMO	
	4.31	0.12	HOMO−4 → LUMO	2.73
			HOMO−3 → LUMO	
			HOMO → LUMO+2	
	4.84	0.17	HOMO−4 → LUMO+1	3.07
			HOMO → LUMO+2	
	5.19	0.21	HOMO−7 → LUMO	3.25
			HOMO−4 → LUMO+1	
			HOMO−3 → LUMO+1	
			HOMO → LUMO+4	
	5.50	0.16	HOMO → LUMO+4	2.77
MPW1PW91	3.30	1.14	HOMO → LUMO	9.53
	4.30	0.14	HOMO−4 → LUMO	2.98
			HOMO−3 → LUMO	
	4.47	0.10	HOMO−4 → LUMO	2.44
			HOMO−3 → LUMO	
			HOMO → LUMO+2	
	5.00	0.17	HOMO−4 → LUMO+1	3.03
			HOMO−3 → LUMO+1	
			HOMO → LUMO+2	
	5.36	0.24	HOMO−4 → LUMO+1	3.44
			HOMO → LUMO+3	
	5.68	0.15	HOMO → LUMO+4	2.67
		Ni Complex		
B3LYP	2.79	1.62	HOMO → LUMO	12.39
	3.18	1.26	HOMO−1 → LUMO+1	10.24
	4.00	0.51	HOMO−6 → LUMO	5.78
			HOMO−5 → LUMO+2	
MPW1PW91	2.97	2.29	HOMO → LUMO	14.27
	3.36	0.77	HOMO−1 → LUMO+1	7.77
	4.26	0.49	HOMO−6 → LUMO	5.49
			HOMO−4 → LUMO+2	

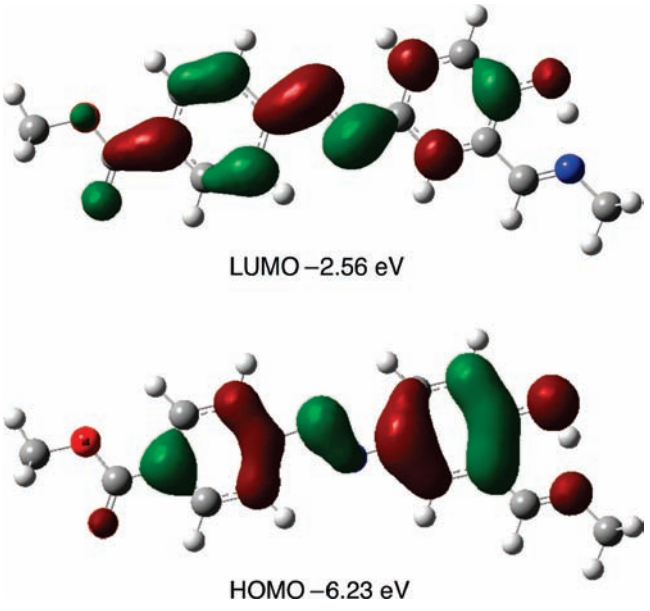

Figure 12. TD-DFT-derived depictions of the main orbitals involved in the ICT transition in the pro-ligand model system obtained by using the MPW1PW91 functional (isosurface value 0.03 au).

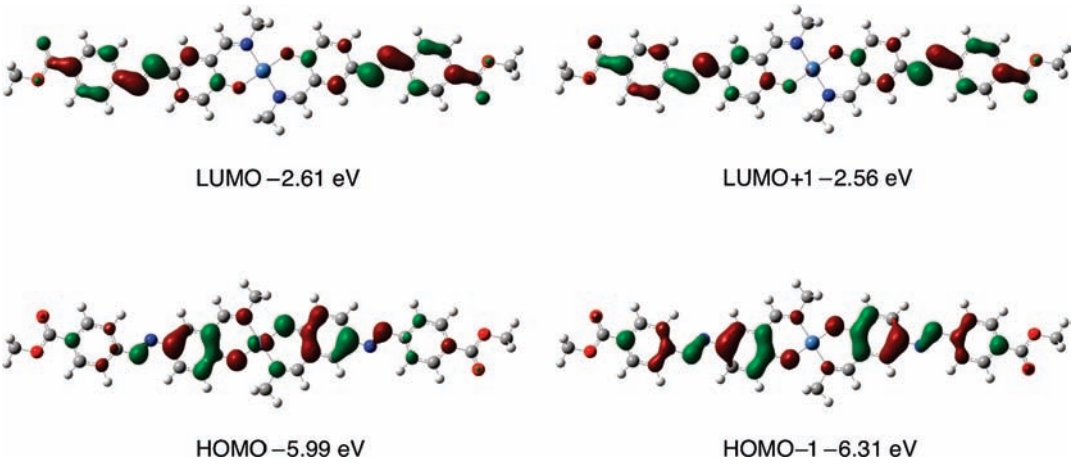

Figure 13. TD-DFT-derived depictions of the main orbitals involved in the ICT transition in the Ni^{II} complex model system obtained by using the B3LYP functional (isosurface value 0.03 au).

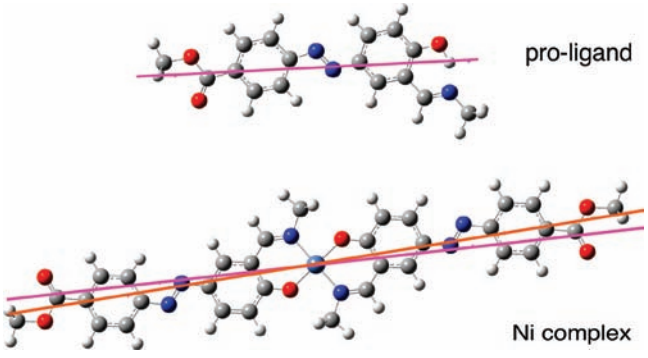

Figure 14. Calculated μ_{12} vectors (scaled to show direction) for the first excited state of the model pro-ligand (MPW1PW91) with $\Delta E = 3.30$ eV (pink) and the first two excited states of the model Ni complex (B3LYP) with $\Delta E = 2.79$ eV (orange) and $\Delta E = 3.18$ eV (pink).

Figure S8). The ICT occurs from orbitals based on the metal center and adjacent rings to the π^* orbitals on the azo unit, with small contributions from other aromatic rings and ester groups. Involvement of the metal in the HOMO is thus supported by these calculations. ZINDO_S calculations using either an optimized geometry or the X-ray crystal structure afford a qualitatively similar picture (Supporting Information, Figures S3 and S5). It is notable that, as with **2eH**, the lowest energy conformation from ZNDDO_2 optimization shows a much greater twist angle between the azobenzene rings (71.7°) than is observed in the solid-state structure (see above). This optimized geometry produces spatially similar high-lying occupied orbitals on ZINDO_S treatment, but the LUMO and LUMO+1 show much greater contribution from orbitals on the ester-substituted ring (Supporting Information, Figure S5).

We have also used TD-DFT calculations to approximate the directions of the transition dipole moments (μ_{12}) for the ICT transitions occurring in the pro-ligand model (using MPW1PW91) and the Ni model complex (using B3LYP). These predictions indicate that the μ_{12} vectors are reasonably well aligned with the long molecular axes in both cases (Figure 14). For the Ni complex, the two transitions composing the visible absorption band give very similar μ_{12} alignment. ZINDO_S calculations with the crystallographically observed structures afford results similar to the TD-DFT predictions (Supporting Information, Figure S9).

Conclusions

We have synthesized a family of N_2O_2-chelated Ni^{II} or Pd^{II} complexes containing azobenzene chromophores, with various substituents close to and remote from the metal center. Single crystal X-ray structures show a trans-square planar arrangement for all of the bis-bidentate chelates, although a slight distortion of the Ni^{II} complexes toward a tetrahedral geometry in solution is evidenced by broadened ^{1}H NMR spectra. Salen-like complexes give sharp ^{1}H NMR spectra, but X-ray crystallography of the Ni^{II} complex reveals a slight distortion in the solid-state. The characteristic azobenzene $\pi \rightarrow \pi^*$ electronic transition gains some degree of MLCT character on complexation of the pro-ligands. Bathochromic shifts of 0.25−0.5 eV are produced which are always larger for the Ni^{II} complexes than for their Pd^{II} analogues, while the extinction coefficients approximately double on complexation. The contribution of the metal to the HOMO in these Ni^{II} complexes is confirmed by ZINDO_S and TD-DFT calculations. These theoretical methods also indicate a good alignment of μ_{12} with the long molecular axis. *DR* measurements on pro-ligands show that a biphenyl unit confers favorable ordering within the LC. While complexation to Ni^{II} increases the *DR*, Pd^{II} complexation of a biphenyl-containing pro-ligand is detrimental. The dichroism of one of the Ni^{II} complexes may be sufficient for potential applications in guest−host displays.

Acknowledgment. We thank the University of Manchester for support and also the EPSRC National Mass Spectrometry Service Centre, Swansea, U.K. We also wish to thank Hewlett-Packard Ltd for the use of the dichrometer and generous donations of LCs.

Supporting Information Available: Crystallographic information in CIF format; further synthetic and characterization details; additional molecular orbital pictures, spectra, and data from TD-DFT calculations on the model compounds and from ZINDO_S studies on the pro-ligand **2eH** and its Ni^{II} complex **3e**; Cartesian coordinates of theoretically optimized geometries; ^{1}H NMR spectra for all new and sufficiently soluble compounds (PDF). This material is available free of charge via the Internet at http://pubs.acs.org.

Note Added after ASAP Publication. This paper was published on the Web on September 14, 2010. Clarification to abbreviations s and st have been made, and the corrected version was reposted on September 20, 2010.